

Testing turbulent closure models with convection simulations

J. E. Snellman¹, P. J. Käpylä^{1,2}, M. J. Mantere¹, M. Rheinhardt¹, and B. Dintrans³

¹ Department of Physics, Gustaf Hållströmin katu 2a (PO Box 64), FI-00014 University of Helsinki, Finland

² NORDITA, Roslagstullsbacken 23, SE-10691 Stockholm, Sweden

³ Observatoire Midi-Pyrénées, Laboratoire d'Astrophysique de Toulouse-Tarbes (UMR5572), 14 Avenue Edouard Belin, 31400 Toulouse, France

Received / Accepted

ABSTRACT

Aims. To compare simple analytical closure models of turbulent Boussinesq convection for stellar applications with direct three-dimensional simulations both in homogeneous and inhomogeneous (bounded) setups.

Methods. We use simple analytical closure models to compute the fluxes of angular momentum and heat as a function of rotation rate measured by the Taylor number. We also investigate cases with varying angles between the angular velocity and gravity vectors, corresponding to locating the computational domain at different latitudes ranging from the pole to the equator of the star. We perform three-dimensional numerical simulations in the same parameter regimes for comparison. The free parameters appearing in the closure models are calibrated by two fit methods using simulation data. Unique determination of the closure parameters is possible only in the non-rotating case and when the system is placed at the pole. In the other cases the fit procedures yield somewhat differing results. The quality of the closure is tested by substituting the resulting coefficients back into the closure model and comparing with the simulation results.

Results. The simulation data for the Reynolds stress and heat fluxes in the homogeneous case broadly agree with previous compressible simulations. The closure works fairly well in the homogeneous case with slow rotation but its quality degrades as the rotation rate is increased. We find that the closure parameters depend not only on Ta but also on latitude. Furthermore, in the inhomogeneous case the closure is unable to reproduce the vertical profiles of the horizontal components of the Reynolds stress.

Key words. hydrodynamics – turbulence – convection – Sun: rotation – stars: rotation

1. Introduction

Turbulent convection is responsible for the transport of angular momentum and heat in stellar convection zones, in particular in that of the Sun. In combination with global rotation, these turbulent flows lead to the generation of large-scale differential rotation and meridional circulation (e.g. Rüdiger 1989), which on the other hand, play key roles in sustaining the dynamo of the Sun (e.g. Krause & Rädler 1980; Rüdiger & Hollerbach 2004).

During the last decades, growing computational resources have allowed direct and large-eddy numerical simulations to reach a level of sophistication where many aspects of the solar differential rotation and dynamo can be captured self-consistently (see, e.g. Miesch et al. 2006; Miesch & Toomre 2009; Ghizaru et al. 2010; Käpylä et al. 2012). However, these simulations are still computationally very expensive and cannot be employed in performing comprehensive parameter surveys. Furthermore, even the currently highest resolution simulations are still far from real stars in parameter space (e.g. Käpylä 2011). An alternate way of dealing with the problem is to parametrize the small scales by turbulent transport coefficients and solve directly only for the large scales. This is often done by approximating higher-order correlations by lower order ones in so-called *closure* approaches. In general the pitfall lies in the limited validity of the analytical approximations under which the results are derived. Hence finetuning of the model parameters is usually required.

A promising approach to the problem is to validate or calibrate the turbulent closure models by comparing their results with direct numerical simulations. However, fairly little has been done to accomplish this in the astrophysical context. This is especially true for closures dealing with turbulent convection (see, however, Garaud et al. 2010).

In this paper we build upon previous studies where simple analytical closure models were compared with simulations of forced or magnetorotationally excited turbulence in fully periodic systems (Käpylä & Brandenburg 2008; Liljeström et al. 2009; Snellman et al. 2009). Here we extend this work to turbulent convection in unstratified Rayleigh–Bénard setups, drawing insights especially from the results of Snellman et al. (2012a,b) (hereafter S12a and S12b) where closure parameters were extracted from forced turbulence simulations. Our aim is to compare three-dimensional direct numerical simulations (DNS) with the closure model for convection put forward by Garaud et al. (2010) (hereafter GOMS10). The bulk of their study is devoted to the derivation and calibration of a closure model for a Boussinesq system. Results of DNS and experiments of bounded and hence inhomogeneous non-rotating Rayleigh–Bénard convection are referred to for the purpose of determining the free parameters of the model. It was found that in the statistically stationary state, to a certain extent universal constants can be extracted which moreover coincide partly with those from a corresponding study of the very different situation of shear flows, see Garaud & Ogilvie (2005).

Similarly, an additional free parameter of the closure for *homogeneous* non-rotating Rayleigh–Bénard convection was esti-

Send offprint requests to: J. E. Snellman
e-mail: jan.snellman@helsinki.fi

mated on the basis of DNS results where its universality turned out to be limited by the destabilization of the fluctuations in shallow computational domains. The predictions of the closure model for the same setup, but with rotation included, were set into relation of previous analytical results. However, no direct comparison with corresponding DNS results was performed, in particular, there was no independent calibration of the model parameters.

The emergence of coherent structures covering the whole vertical extent of the domain was quite generally pointed out to be limiting the validity of the essentially *local* closure. For the case of rotating homogeneous Rayleigh-Bénard convection a further limit was found in the independence of the closure model on the rotation rate when gravitation and rotation are perfectly aligned.

Hence, the goal of the present paper is to scrutinize the potential of the GOMS10 closure model for rotating convection, both for the case of homogeneous and inhomogeneous Boussinesq convection.

2. Models and methods

2.1. The Boussinesq system

2.1.1. Basic equations

We consider a closure model for Boussinesq convection both in a plane layer and infinitely extended space following the pattern of Miller & Garaud (2007) and GOMS10. In general, the time evolution of the velocity and temperature fields is governed by the Navier-Stokes, continuity, and heat transfer equations

$$\rho \frac{DU}{Dt} = -\nabla p + \rho(\mathbf{g} - 2\boldsymbol{\Omega} \times \mathbf{U} + \mathbf{f}_{\text{visc}}), \quad (1)$$

$$\frac{D \ln \rho}{Dt} = -\nabla \cdot \mathbf{U}, \quad (2)$$

$$\rho c_V \frac{DT}{Dt} = \nabla \cdot K \nabla T - p \nabla \cdot \mathbf{U} + 2\nu \rho \mathbf{S}^2, \quad (3)$$

where \mathbf{U} is the velocity, ρ is the density, \mathbf{g} is the gravitational acceleration, \mathbf{f}_{visc} is the viscous force per mass, p is the pressure, T is the temperature, c_V is the specific heat at constant volume, K is the heat conductivity and $D/Dt = \partial/\partial t + \mathbf{U} \cdot \nabla$ denotes the advective derivative. In the following, we assume that \mathbf{g} and c_V have constant values. The viscous force is given by

$$\mathbf{f}_{\text{visc}} = \nu \left(\nabla^2 \mathbf{U} + \frac{1}{3} \nabla \nabla \cdot \mathbf{U} + 2 \mathbf{S} \cdot \nabla \ln \rho \right), \quad (4)$$

with the kinematic viscosity ν assumed constant and the traceless rate of strain tensor \mathbf{S} , which can be written in component form as

$$S_{ij} = \frac{1}{2} (\partial_j U_i + \partial_i U_j) - \frac{1}{3} \delta_{ij} \partial_k U_k. \quad (5)$$

In the Boussinesq approximation, convection is understood as a perturbation to a stationary, purely conductive reference state with constant density ρ_0 which is hence governed by

$$0 = -\nabla p_0 + \rho_0 \mathbf{g}, \quad 0 = \chi \nabla^2 T_0 + q_0, \quad (6)$$

where the thermal diffusivity $\chi = K/\rho c_V$ is assumed to be constant and a stationary heat source q_0 can be included. In this paper, however, we rely on the simplest case with $q_0 = 0$ and a consequently uniform temperature gradient ∇T_0 enforced by appropriate boundary conditions. Denoting the deviations of density, pressure and temperature from their reference values caused by convection by ρ' , p' and Θ , respectively, that is, $\rho = \rho_0 + \rho'$,

$p = p_0 + p'$ and $T = T_0 + \Theta$, we obtain from (2) and (6) for the momentum balance

$$\rho_0 \frac{DU}{Dt} = -\nabla p' + \rho' \mathbf{g} - 2\rho_0 \boldsymbol{\Omega} \times \mathbf{U} + \rho_0 \mathbf{f}_{\text{visc}}. \quad (7)$$

According to the key idea of the Boussinesq approximation, the density deviation ρ' from its reference value ρ_0 is assumed to be negligible *except in the buoyancy force* $\rho \mathbf{g}$. Density and temperature perturbations are interconnected by

$$\frac{\rho'}{\rho_0} = -\alpha(T - T_0) = -\alpha\Theta, \quad (8)$$

where α is the coefficient of thermal volume expansion. Finally, the equations of the Boussinesq approximation read

$$\begin{aligned} \frac{DU}{Dt} &= -\nabla \Psi - \alpha \Theta \mathbf{g} - 2\boldsymbol{\Omega} \times \mathbf{U} + \nu \nabla^2 \mathbf{U}, \quad \nabla \cdot \mathbf{U} = 0 \\ \frac{D\Theta}{Dt} &= \chi \nabla^2 \Theta - \mathbf{U} \cdot \nabla T_0. \end{aligned} \quad (9)$$

Here, the reduced pressure $\Psi = p'/\rho_0$ was introduced and the viscous force was simplified for the now incompressible flow. Contributions to heat transfer from viscous heating and compression work are omitted for simplicity.

2.1.2. Domain, boundary conditions, control parameters

For the computational domain we consider a rectangular box thought of being cut out at a varying latitude from the convection zone of a rotating star. We choose Cartesian coordinates (x, y, z) such that their directions locally correspond to those of the global spherical coordinates (ϑ, ϕ, r) having their axis $\vartheta = 0$ aligned with the angular velocity vector $\boldsymbol{\Omega}$. In (9) the latter has then to be written as

$$\boldsymbol{\Omega} = \Omega_0 (-\sin \vartheta, 0, \cos \vartheta)^T, \quad (10)$$

where ϑ is the colatitude. We will let the box adopt seven different positions defined by varying ϑ in equidistant steps of 15 degrees from 0° (pole) to 90° (equator). For the dimensions of the box, L_x, L_y, L_z , we assume $L_x = L_y$ while L_z may differ from them.

For all quantities, periodic boundary conditions in the horizontal (x, y) directions are employed throughout the paper. For the conditions at the z boundaries we adopt a combination of non-penetrating stress-free flow/zero temperature perturbation, i.e.

$$\partial_z U_x = \partial_z U_y = U_z = \Theta = 0 \quad \text{at} \quad z = 0, L_z \quad (11)$$

or periodic conditions for all quantities. While in the former case the constant reference temperature gradient ∇T_0 is given by the reference temperature difference across the layer, it has to be considered an independent parameter of the equations (9) in the latter. The non-periodic case shows the complication of the convective turbulence becoming inhomogeneous near the boundaries. In contrast, the periodic case does not feature any causes for inhomogeneity and is therefore also labelled as *homogeneous Rayleigh-Bénard convection*. In both cases the turbulence naturally has to exhibit anisotropy already because of the preference of the gravity, i.e., the z direction.

The system (9) is governed by the following three dimensionless parameters: The magnitude of the temperature gradient (and eventually the vigour of the convection) is quantified by the Rayleigh number

$$\text{Ra} = \frac{\alpha g d^3 \Delta T_0}{\nu \chi}, \quad (12)$$

where $g = g_z$, ΔT_0 is the reference temperature difference between the top and the bottom of the domain and $d = L_z$ its vertical extent. For the case of periodicity in z , the definition (12) has to be modified properly employing the constant background temperature gradient $\nabla_z T_0 = G_0$, that is

$$\text{Ra} = \frac{\alpha g d^4 G_0}{\nu \chi}. \quad (13)$$

The ratio of viscosity and thermal diffusivity is given by the Prandtl number

$$\text{Pr} = \frac{\nu}{\chi}, \quad (14)$$

and finally the rotation rate is measured by the Taylor number

$$\text{Ta} = \frac{4\Omega^2 d^4}{\nu^2}. \quad (15)$$

Another way to express the strengths of rotation and viscous effects, but in the form of diagnostics rather than of control parameters, is provided by the Coriolis and Reynolds numbers, respectively,

$$\text{Co} = \frac{2\Omega_0}{U_{\text{rms}} k_f}, \quad \text{Re} = \frac{U_{\text{rms}}}{\nu k_f}, \quad (16)$$

where $k_f = 2\pi/d$ is the wave number corresponding to the vertical extent d and $U_{\text{rms}} = (\int_V U^2 dV/V)^{1/2}$ is the root mean square velocity with the volume of the domain V .

2.1.3. Closure model

In deriving the closure model we first have to specify the averaging procedure by which the mean quantities are defined. Given the periodicity of our models in the horizontal directions, averaging over these directions is appropriate and we will apply it throughout this paper. Hence, the mean of a quantity f , indicated by an overbar, is given by $\overline{f}(z) = \int_{L_x} \int_{L_y} f(x, y, z) dx dy / L_x L_y$. This procedure satisfies all the Reynolds averaging rules. Denoting turbulent quantities with lowercase letters, we have $\mathbf{U} = \overline{\mathbf{U}} + \mathbf{u}$, $\Theta = \overline{\Theta} + \theta$ etc. and the equations for the mean quantities read

$$\nabla \cdot \overline{\mathbf{U}} = 0, \quad (17)$$

$$\frac{\partial \overline{\mathbf{U}}}{\partial t} = -\overline{\mathbf{U}} \cdot \nabla \overline{\mathbf{U}} - \alpha \overline{\Theta} \mathbf{g} - \nabla \overline{\Psi} - 2\Omega \times \overline{\mathbf{U}} + \nu \nabla^2 \overline{\mathbf{U}} - \nabla \cdot \mathcal{R}, \quad (18)$$

$$\frac{\partial \overline{\Theta}}{\partial t} = -\overline{\mathbf{U}} \cdot \nabla (T_0 + \overline{\Theta}) + \chi \nabla^2 \overline{\Theta} - \nabla \cdot \mathcal{F}, \quad (19)$$

where \mathcal{R} is the Reynolds stress tensor, $\mathcal{R}_{ij} = \overline{u_i u_j}$, and \mathcal{F} is the turbulent heat flux, $\mathcal{F}_i = \overline{\theta u_i}$. These equations are identical to those used in GOMS10, with the exception of the extra Coriolis term. As a consequence of the chosen average, horizontal derivatives vanish and the continuity equation reduces to $\partial_z \overline{U}_z = 0$, from which it follows that $\overline{U}_z = \text{const}$. For the plane layer with impenetrable boundaries this means $\overline{U}_z = 0$. The equations for the remaining components of the mean velocity read, with gravity having only a z component,

$$\dot{\overline{U}}_x = -\partial_z \mathcal{R}_{xz} + 2\Omega_z \overline{U}_y + \nu \partial_{zz} \overline{U}_x, \quad (20)$$

$$\dot{\overline{U}}_y = -\partial_z \mathcal{R}_{yz} + 2(\Omega_x \overline{U}_z - \Omega_z \overline{U}_x) + \nu \partial_{zz} \overline{U}_y.$$

Note that we do not need to solve for the mean pressure $\overline{\Psi}$ as it would only affect \overline{U}_z . The equation for $\overline{\Theta}$ reduces to

$$\dot{\overline{\Theta}} = \chi \partial_{zz} \overline{\Theta} - \partial_z \mathcal{F}_z. \quad (21)$$

Evolution equations for the Reynolds stress and turbulent heat flux can be derived from the equations for the turbulent quantities \mathbf{u} and θ , see Appendix A. In doing so one comes inevitably across higher-order correlations of u_i and θ . The essential step of the closure procedure as proposed in GOMS10 consists then in replacing these correlations by aggregates of second-order correlations, more specifically, of the quantities \mathcal{R} and \mathcal{F} themselves. In an analogous way, some second-order correlations which cannot directly be expressed by the components of \mathcal{R} and \mathcal{F} , or \mathcal{Q} are modelled. The details can again be found in Appendix A. In their final form the closed set of equations reads

$$\dot{\mathcal{R}}_{ij} + \overline{U}_k \partial_k \mathcal{R}_{ij} + \mathcal{R}_{ik} \partial_k \overline{U}_j + \mathcal{R}_{jk} \partial_k \overline{U}_i + \alpha (\mathcal{F}_i g_j + \mathcal{F}_j g_i) - \nu \partial_{kk} \mathcal{R}_{ij} + 2\Omega_l (\varepsilon_{ilk} \mathcal{R}_{jk} + \varepsilon_{jlk} \mathcal{R}_{ik}) \quad (22)$$

$$= - \left(\frac{C_1 + C_2}{L} \mathcal{R}^{1/2} + \nu \frac{C_\nu}{L^2} \right) \mathcal{R}_{ij} + \frac{C_2}{3L} \mathcal{R}^{3/2} \delta_{ij},$$

$$\dot{\mathcal{F}}_i + \overline{U}_j \partial_j \mathcal{F}_i + \mathcal{F}_j \partial_j \overline{U}_i + \mathcal{R}_{ij} \partial_j (\overline{\Theta} + T_0) + \alpha \mathcal{Q} g_i - \frac{1}{2} (\nu + \chi) \partial_{jj} \mathcal{F}_i + 2\varepsilon_{ijk} \Omega_j \mathcal{F}_k \quad (23)$$

$$= - \left(\frac{C_6}{L} \mathcal{R}^{1/2} + \frac{1}{2} (\nu + \chi) \frac{C_{\nu\chi}}{L^2} \right) \mathcal{F}_i,$$

where $\mathcal{R} = \mathcal{R}_{xx} + \mathcal{R}_{yy} + \mathcal{R}_{zz}$ is the trace of \mathcal{R} , $\mathcal{Q} = \overline{\theta^2}$ is the temperature variance, $C_{1,2,6,7,\nu,\nu\chi,\chi}$ are the model parameters and L is a characteristic length scale, here taken to be the distance to the closest boundary, $L = \min(z, d - z)$. Hence, the closure terms are explicitly position dependent. In order to obtain a closed system of equations, (20)–(23) have to be completed by an additional one for \mathcal{Q} which can be derived using Eq. (9). With a closure applied in the same way as for \mathcal{R} and \mathcal{F} , it can be written as

$$\dot{\mathcal{Q}} + \overline{U}_i \partial_i \mathcal{Q} + 2\mathcal{F}_i \partial_i (\overline{\Theta} + T_0) - \chi \partial_{ii} \mathcal{Q} = - \left(\frac{C_7}{L} \mathcal{R}^{1/2} - \chi \frac{C_\chi}{L^2} \right) \mathcal{Q}. \quad (24)$$

As for the original problem, we assume stress-free impenetrable vertical boundaries at $z = 0, d$ for the mean velocity and given that corresponding conditions hold for the turbulent velocity \mathbf{u} , we may require

$$\partial_z \mathcal{R}_{xx} = \partial_z \mathcal{R}_{xy} = \partial_z \mathcal{R}_{yy} = \mathcal{R}_{xz} = \mathcal{R}_{yz} = \mathcal{R}_{zz} = 0, \quad (25)$$

although the first three are only necessary, but not sufficient. Given that the temperature T is fixed at the boundaries, the perturbation Θ and with it both $\overline{\Theta}$ and θ must vanish there. Thus the boundary conditions for mean temperature perturbation, turbulent heat flux and temperature variance are

$$\overline{\Theta} = \mathcal{F}_x = \mathcal{F}_y = \mathcal{F}_z = \mathcal{Q} = 0. \quad (26)$$

For homogeneous turbulence which is obtained in the fully periodic setup, the closure model can be further simplified by defining mean quantities as volume averages over all space or, what is the same, over the computational domain. Then the second-order correlations \mathcal{R}_{ij} , \mathcal{F}_i , \mathcal{Q} are completely decoupled from the mean fields $\overline{\mathbf{U}}$ and $\overline{\Theta}$ and for the latter only trivial

solutions exist, see (20) and (21). The remaining set of ordinary differential equations with respect to time is provided in Appendix B, see also GOMS10, Sect. 4.4. Note that now there is no longer an argument to identify the length scale L in the closure ansatzes with the distance to the nearest boundary, as the periodic boundaries do not limit structure formation. We have chosen to identify L with the vertical extent of the computational box (the fundamental period of the considered fields in z), but it could also be considered a free parameter. Anyway, by comparison with DNS or experiments only the combinations $C_{1,2,6,7}/L$ and $C_{\nu,\nu\chi,\chi}/L^2$ can be determined.

2.2. DNS setups

For the DNS two different setups are used, both in a local Cartesian volume of size $L_x \times L_y \times L_z$: a fully periodic setup with a uniform background temperature gradient as described in Sec. 2.1 for the homogeneous case, and an inhomogeneous setup where either stress-free

$$\partial_z U_x = \partial_z U_y = U_z = 0, \quad (27)$$

or no-slip

$$U_x = U_y = U_z = 0, \quad (28)$$

boundary conditions are applied for the velocity. The temperature is kept fixed at the vertical boundaries. In the inhomogeneous setup the aspect ratio of the box is five, i.e. $L_x = L_y = 5L_z$, whereas it is one in the homogeneous setup.

The numerical simulations were performed with the PENCIL CODE¹, which uses sixth-order accurate finite differences in space, and a third-order accurate time-stepping scheme, see Brandenburg & Dobler (2002); Brandenburg (2003). In all cases the time integration was advanced until a statistically stationary state was reached. In addition to the horizontal or volume averages, a time average over this state is taken because in particular in the homogeneous case the spatial averages still show strong fluctuations. Errors are estimated by dividing the time series into three equally long parts and computing mean values for each part individually. The largest departure from the mean value computed for the whole time series is taken to represent the error.

3. Results

GOMS10 stated strong rotation to be an effect that could possibly reduce or completely rule out the applicability of the closure. The onset of convection and its saturated stage as a function of rotation were studied by Miller & Garaud (2007) using essentially the same closure model as that in GOMS10, but they did not directly compare mean quantities like \mathcal{R} from the model with the corresponding ones from DNS. Hence it is the main purpose of this paper to study the behavior of the GOMS10 model for a range of rotation rates (or Taylor numbers) and for different inclinations of the rotation axis by performing such comparisons.

3.1. DNS Runs

The homogeneous runs are summarised in Table 1, for more details see Table B.1 in the Online Material. In each of the sets

Table 1: Summary of the homogeneous DNS runs at different colatitudes ϑ . $Ra = 3 \cdot 10^5$ and $Pr = 1$ throughout. $Ta = 4 \cdot 10^4 \dots 1.3 \cdot 10^7$ in sets A through G.

Set	ϑ	Re	Co	$U_{\text{rms}}/(d\alpha g \Delta T_0)^{1/2}$
Z		91	0	0.57
A	0°	91 – 127	0.06 – 0.87	0.57 – 0.80
B	15°	81 – 91	0.06 – 1.09	0.51 – 0.57
C	30°	70 – 89	0.06 – 1.07	0.44 – 0.56
D	45°	62 – 91	0.06 – 1.39	0.39 – 0.57
E	60°	57 – 96	0.06 – 0.95	0.36 – 0.61
F	75°	54 – 89	0.06 – 1.02	0.34 – 0.54
G	90°	48 – 85	0.06 – 1.22	0.30 – 0.54

A–G the latitude was kept fixed, but the rotation rate was varied. Z denotes the non-rotating run. The ranges for the Reynolds and Coriolis numbers as well as the rms velocity U_{rms} probed by DNS are listed.

In the homogeneous DNS runs we had to deal with a numerical stability problem in the transition from the kinematic, exponentially growing, stage to the stationary stage if the Taylor number was too small. To circumvent this we started the runs with high ($\approx 10^7$) values of Ta which allowed a statistically stationary state to be established. Then we gradually lowered Ta until the desired parameter range had been reached. Eventually we were able to successfully perform even a non-rotating run using this method. A snapshot of the vertical velocity in this Run Z is pictured in the left panel of Fig. 1. In the time series of the statistically stationary state, we observe large fluctuations and intermittent exponential growth, most likely as a manifestation of the so-called “elevator modes”, described in Calzavarini et al. (2006), which are weakly damped for a box aspect ratio of unity

As a more realistic example, we performed simulations with an inhomogeneous setup with the similar values of Ra and Pr as in the homogeneous runs. The distribution of the velocity component U_z of a non-rotating DNS run with stress-free boundary conditions is shown in Fig. 1, right panel. One can immediately see that there are flow patterns encompassing the entire vertical span of the simulation box. As the closure ansatzes in (22)–(24) are local in space and time, the presence of such large-scale coherent structures can adversely affect their applicability, as already noted by GOMS10.

3.2. Homogeneous case

3.2.1. Calibration of the closure model

We assume that the Rayleigh numbers are high enough so that we can set $C_\nu = C_{\nu\chi} = C_\chi = 0$ throughout. This is probably justified in the case of the homogeneous setup where no boundary layers are present although a parameter scan in Ra would be required to ascertain this for sure. In the inhomogeneous case this is less clear. However, apart from boundary layers there are other more serious issues that affect the results and that will be described in Sect. 3.3. Stationary solutions of the closure model, Eqs. (B.1) in Appendix B, result for given $\{C_i\}$ from the corresponding nonlinear *algebraic* system of equations. This opens up systematic ways of calibrating the parameters. Two such methods are described here.

¹ <http://code.google.com/p/pencil-code/>

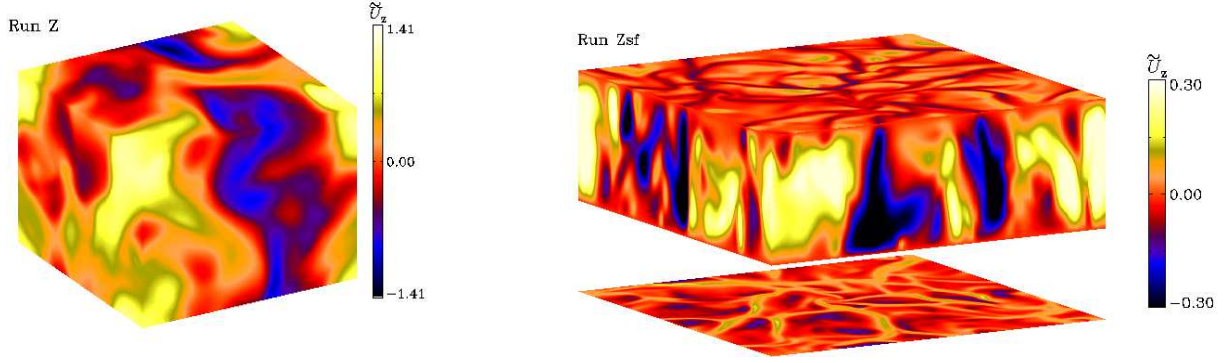


Fig. 1: Velocity component U_z in units of $(\alpha g \Delta T_0)^{1/2}$ from non-rotating DNS runs. Left: homogeneous case Run Z, $Ra = 3 \cdot 10^5$; right: inhomogeneous case Run Zsf, with stress-free vertical boundaries, $Ra = 5 \cdot 10^5$.

Least squares fit By inserting the parameters $(\alpha g, \Omega_0, G_0)$ used in the DNS runs together with their statistically stationary results for \mathcal{R} , \mathcal{F} and \mathcal{Q} into the stationary version of the closure equations (B.1), a generally overdetermined system of linear equations for the $C_{1,2,6,7}$ (ten equations vs. four variables) of the form

$$\mathbf{N}\mathbf{c} = \mathbf{L} \quad (29)$$

is obtained where $\mathbf{c} = (C_1, C_2, C_6, C_7)$. The matrix \mathbf{N} can be derived from the closure terms and the vector \mathbf{L} contains all remaining terms, such as the Coriolis and buoyancy terms, see Eqs. (B.1). At the pole, however, the system (29) is no longer overdetermined and \mathbf{c} can be determined unambiguously as demonstrated in Appendix B. At all other latitudes this system can be solved only approximately using the standard linear least squares method, that is, solving the regular system $\mathbf{N}^T \mathbf{N} \mathbf{c} = \mathbf{N}^T \mathbf{L}$, where the superscript ‘‘T’’ denotes transposition. The results from this procedure are shown in Fig. 2 as functions of Taylor number and colatitude. As an indicator of the quality of the solution, we also calculated the residual norm

$$\text{Res}_{\mathbf{L}} = \|\mathbf{N}\mathbf{c}_{\text{ls}} - \mathbf{L}\|, \quad (30)$$

where the subscript ‘‘ls’’ refers to the least-squares solution and $\|\cdot\|$ denotes the Euclidian norm, see Fig. 2. Another way to quantify the quality of the obtained closure model consists in calculating the difference in the stationary solutions for $\mathbf{X} = (\mathcal{R}_{xx}, \dots, \mathcal{R}_{zz}, \mathcal{F}_x, \mathcal{F}_y, \mathcal{F}_z, \mathcal{Q})$ from the closure model (B.1) with $\mathbf{c} = \mathbf{c}_{\text{ls}}$ and from the corresponding temporally averaged results of the DNS run, that is, calculating the residual

$$\text{Res}_{\mathbf{X}} = \|\mathbf{X}_{\text{closure}} - \mathbf{X}_{\text{DNS}}\|. \quad (31)$$

This quantity is also shown in Fig. 2 together with the left hand side of the realizability condition

$$2C_6 - C_7 - C_1 - C_2 \geq 0 \quad (32)$$

given in GOMS10 and the largest eigenvalue of the linearized system, see below. The solutions $\mathbf{X}_{\text{closure}}$ and \mathbf{X}_{DNS} are directly compared in Fig. 3. When Eq. (29) is overdetermined, there is in general not any set of coefficients $\{C_i\}$ with which the closure reproduces all the modeled quantities perfectly. This is indicated by the residual (31).

From Fig. 2 one can see that the derived model coefficients change with colatitude and Taylor number, with following patterns: at the pole they fall with growing Ta, but not so for any other colatitude. Instead, they first grow with Ta and plateau or

Table 2: Ratios of the coefficients C_i obtained from the non-rotating Run Z compared to GOMS10 and S12a,b.

C_i/C_j	this study	S12a	S12b	GOMS10
C_1/C_2	0.82	≈ 0.4	—	0.66
C_1/C_6	0.42	—	—	0.29
C_1/C_7	0.58	—	—	0.29
C_2/C_6	0.51	—	—	0.43
C_2/C_7	0.72	—	—	0.43
C_6/C_7	1.40	—	≈ 2.1	1.00

fall for $Ta > 10^6$. Both growth and fall get steeper with growing colatitude, and all the curves converge as Ta approaches zero.

Using the (exact) results for the non-rotating run we computed the different ratios of the coefficients $\{C_i\}$ and compared them to the corresponding ratios from GOMS10, S12a, and S12b in Table 2. These ratios are important because any difference in the non-rotating case in the results for C_i could be due to a badly chosen lengthscale L , which is canceled by the ratios. In any case, we see that our values are at odds with those of GOMS10. As for the residuals, they unsurprisingly vanish (up to round-off errors) at the pole, otherwise rise with Taylor number while the colatitude has only a small effect on the residual (30), but a stronger one on (31). At the equator the residual $\text{Res}_{\mathbf{X}}$ settles at unity for $Ta \gtrsim 5 \cdot 10^7$. This is because the analytical results from the closure become very small for all the modeled quantities indicating that the obtained $\{C_i\}$ do not allow for another than the trivial solution of (B.1).

The DNS results \mathbf{X}_{DNS} for a slow and a rapid rotation case are compared with the corresponding closure results obtained with the derived model coefficients in Fig. 3. At slow rotation the DNS and the closure results are visibly closer to each other than at fast rotation. Further, the fit for small quantities like $\mathcal{R}_{xy,xz,yz}$ or $\mathcal{F}_{x,y}$ is significantly worse than for the large ones, like \mathcal{R}_{zz} , \mathcal{F}_z or \mathcal{Q} . This is mainly because residuals of large quantities contribute stronger to the norm of the residual vector which is minimized by the least squares method.

Optimization approach In order to determine the $\{C_i\}$ from the results of the DNS in an optimum way, we can also formulate the following optimization problem: minimize the *objective*

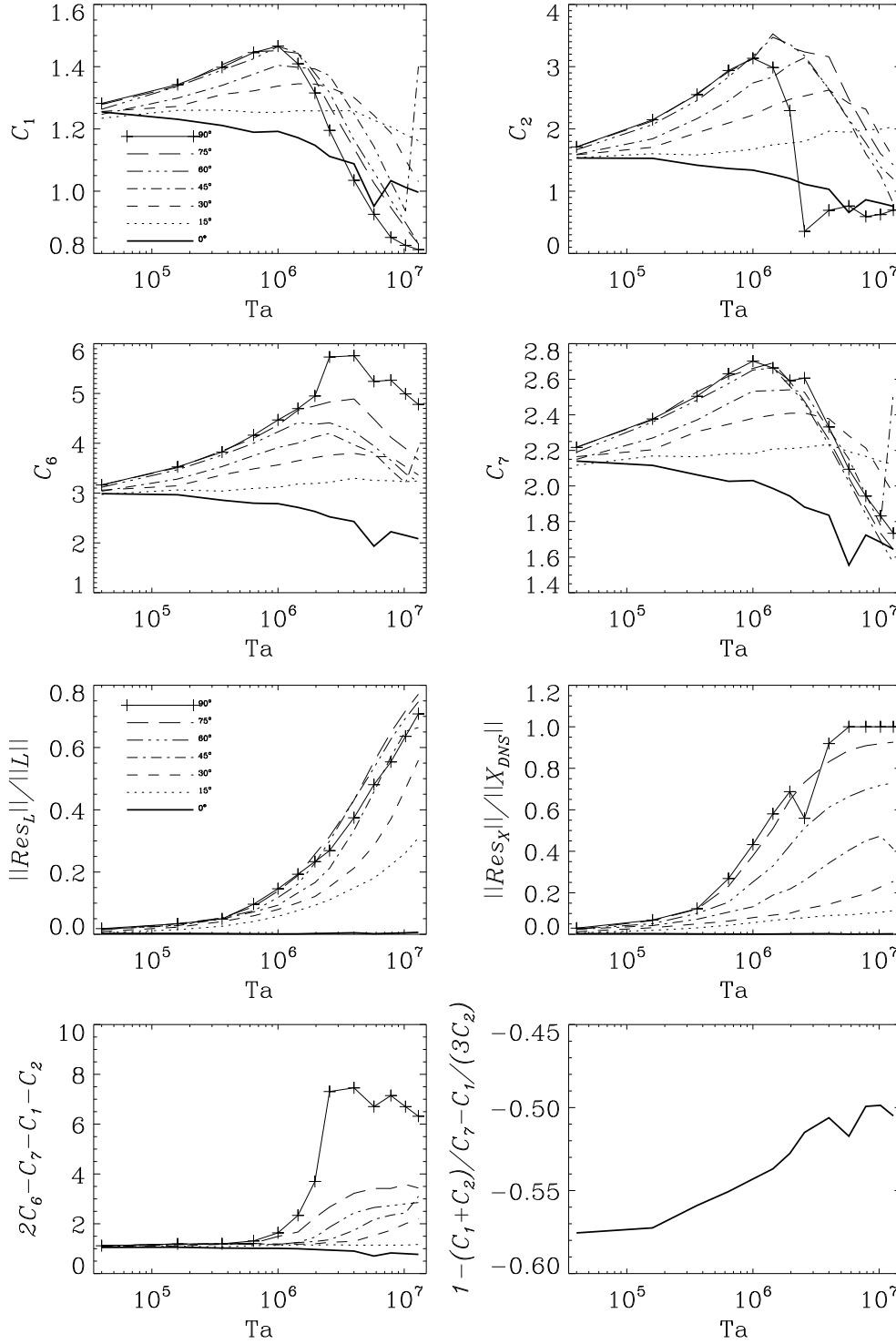


Fig. 2: Closure parameters from the least-squares approach. Upper four panels: $\{C_i\}$ as functions of Ta ; Third row of panels: normalized residuals (30) and (31). Lowest two panels: values of the constraint (32) and largest eigenvalue of the linearized system (for $\vartheta = 0$ only).

function

$$(\mathbf{X}_{\text{closure}} - \mathbf{X}_{\text{DNS}})^2 \quad (33)$$

obeying the constraints $C_{1,2,6,7} > 0$ and (32). The problem was solved by the Generalized Reduced Gradient Method (Lasdon et al. (1978)) as implemented by the IDL routine `CONSTRAINED_MIN` with the nonlinear system from Eqs. (B.1) being solved by Newton iteration (IDL routine

NEWTON). The optimum results are shown in Fig. 4 where the upper four panels refer to the $\{C_i\}$ while the lower left one gives the normalized objective function

$$(\mathbf{X}_{\text{closure}} - \mathbf{X}_{\text{DNS}})^2 / \mathbf{X}_{\text{DNS}}^2 \quad (34)$$

and the lower right one the value of the quantity $2C_6 - C_7 - C_1 - C_2$ from the constraint (32). Along with the dependence on Ta ,

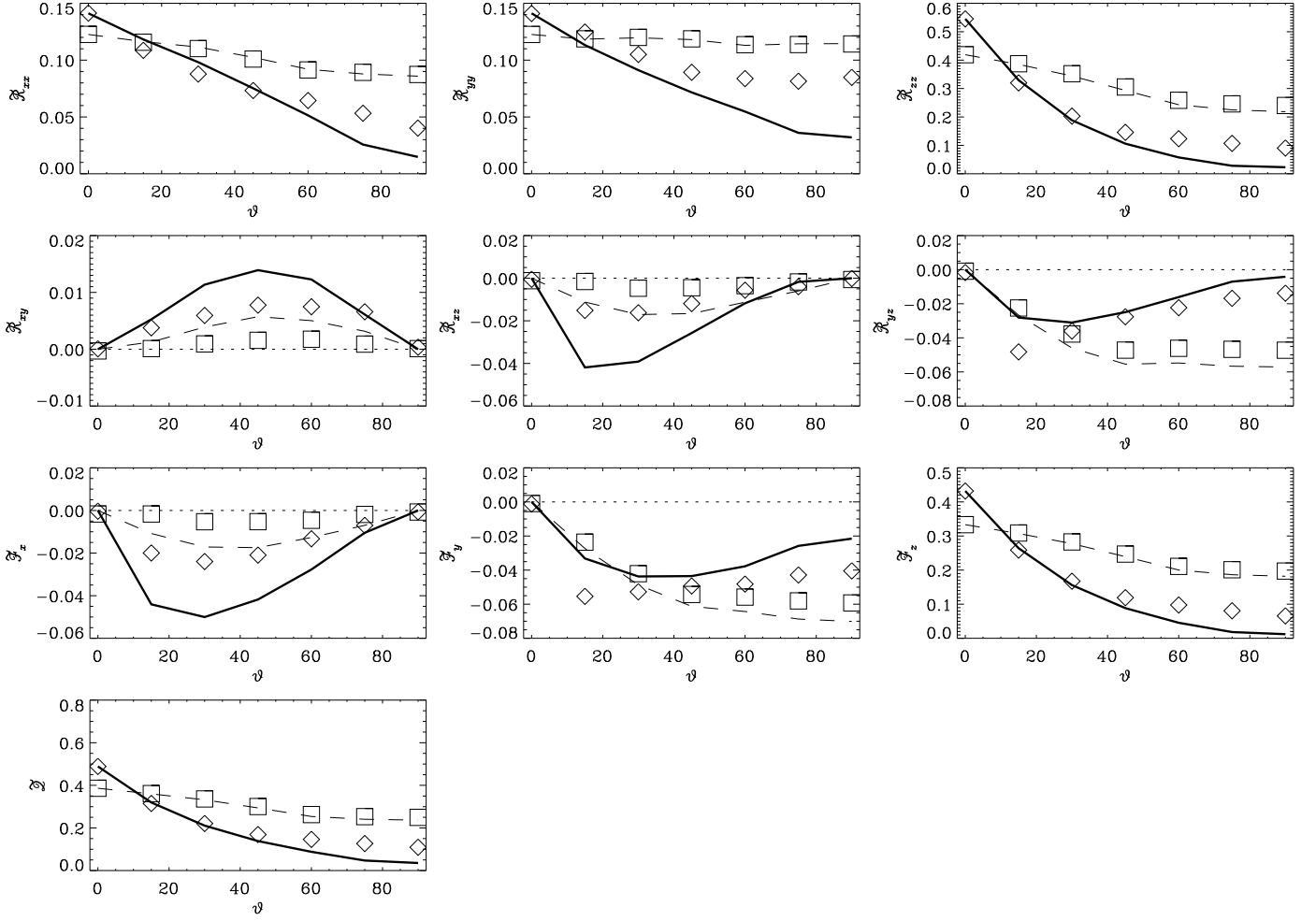


Fig. 3: Results of the closure model with coefficients $\{C_i\}$ from the least squares fit compared with the corresponding DNS results. Note that the $\{C_i\}$ depend on rotation rate Ω_0 and colatitude ϑ , see Fig. 2. Dotted lines/squares: closure/DNS results for slow rotation (Runs A2–G2 with $Ta = 1.6 \cdot 10^5$), solid lines/diamonds: for faster rotation (Runs A7–G7 with $Ta = 1.96 \cdot 10^6$).

there is again in general a separate one on ϑ . At the pole ($\vartheta = 0$) the objective function assumes exceptionally low values. This is a consequence of the already mentioned degeneration which allows to determine the $\{C_i\}$ uniquely from the \mathbf{X}_{DNS} . Hence the objective function actually vanishes and the observed values are completely due to the iterative nature of the solution and round-off errors. Apart from the pole, the quality of the optimum is in general decreasing with growing Ta , yet having only a weak dependence on colatitude. For $10^6 \leq Ta \leq 1.6 \cdot 10^7$ and Ta dependent ϑ intervals between 45° and 75° , the constraint (32) becomes “active” in the sense that the optimum lies then on the margin of the admissible domain, that is, $2C_6 - C_1 - C_2 - C_7 = 0$ (red curve sections in Fig. 4).

Given that, apart from the constraint (32), also the stability properties of the closure model should not differ from that of the DNS, we enhanced the optimization problem by the constraint that for the optimum fit the stationary solution corresponding to it should be stable. For that, we linearized the system (B.1) about the state $\mathbf{X}_{\text{closure}}$, obtaining a system of the form $\partial_t(\delta\mathbf{X}) = \mathbf{A} \cdot \delta\mathbf{X}$ for the perturbations $\delta\mathbf{X}$, and required that the maximum of the real parts of the eigenvalues of \mathbf{A} is negative. To avoid influences of numerical noise we set their upper bound to a small negative value instead of zero. The matrix eigenvalue problem was solved by means of the IDL routines

LA_ELMHES and LA_HQR. It turned out that the additional constraint never becomes active, that is, that stability is already granted if only (32) is obeyed.

In Fig. 5 the DNS and closure model results as functions of the colatitude are given for two different Taylor numbers. Obviously, the dominant variables R_{zz} , F_z and Q are always acceptably fitted. For slow rotation, also the other quantities except R_{yz} show good fits. By applying appropriate weights in the objective function (33) the fit quality could be distributed “more equally”, but such a procedure suffers from high arbitrariness.

Both versions of the optimization approach produce up to roundoff errors identical results as long as neither of the two constraints is active. The dependence of the objective function on latitude is in general weak, and beyond $Ta \approx 10^7$ its dependence on Ta is weak too. Again, the ratios C_1/C_2 and C_6/C_7 for the non-rotating case are at odds with GOMS10, see Table 3. When comparing the results of the least-squares and the optimization approaches we find major quantitative differences in $C_{1,2,7}$, in addition differing monotony in $C_{1,7}$ while the residuals are clearly smaller for the latter approach, namely $\approx 30\%$ vs. up to 100 % for the former.

Dependence on Ta For both approaches, the obtained $\{C_i\}$ show a strong dependence on Ta . At the pole, however, there is

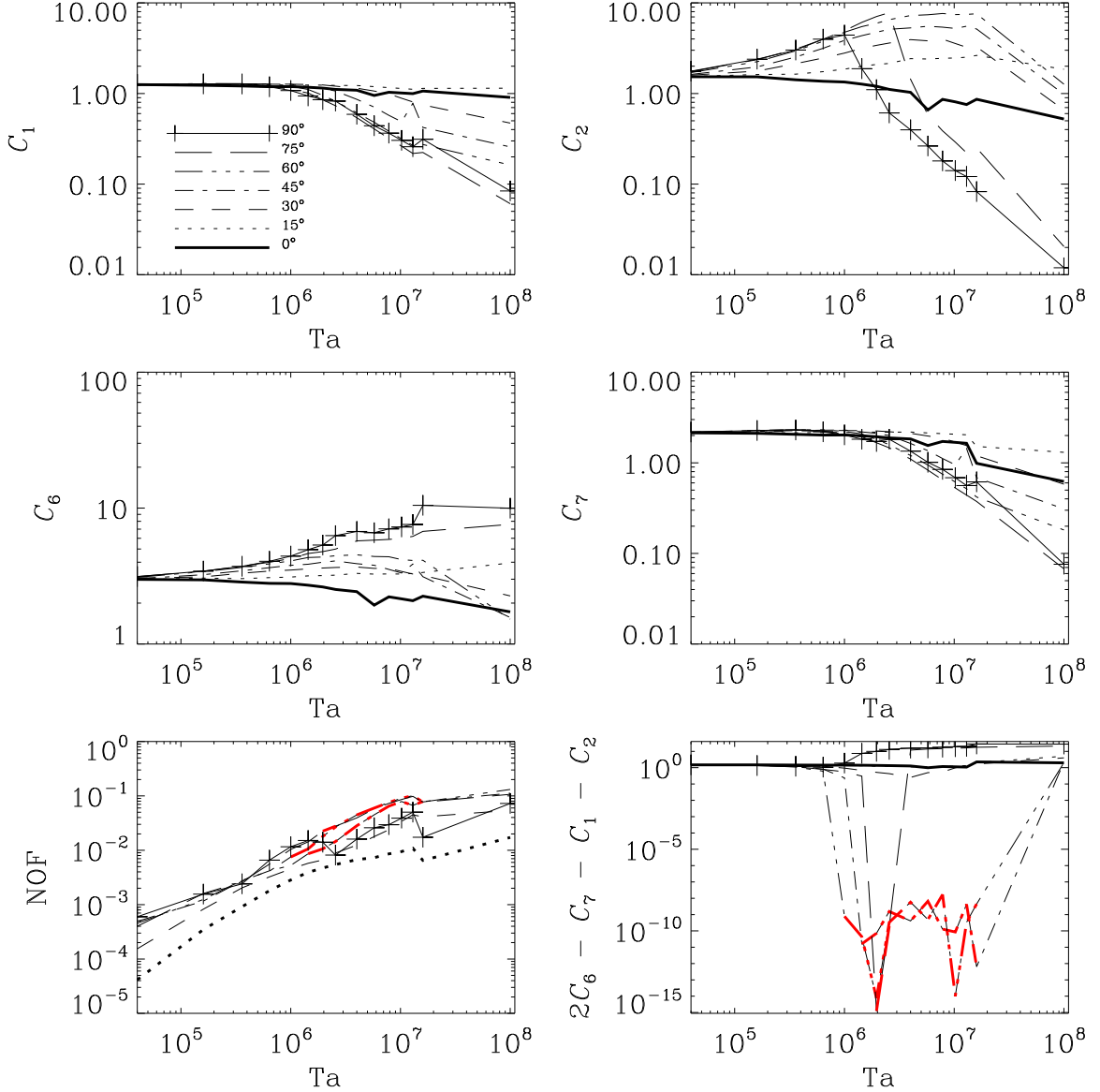


Fig. 4: Closure parameters from the optimization approach. Upper four panels: $\{C_i\}$ as functions of Ta . Lower left panel: normalized objective function (34) at optimum (NOF); values for $\vartheta = 0^\circ$ are omitted because they reflect only roundoff errors. Lower right: value of $2C_6 - C_7 - C_1 - C_2$ from (32). Red: Regions in which the constraint is active.

Table 3: Ratios of the coefficients C_i obtained for rotating runs by the optimization approach. $Ta = 4 \cdot 10^4 \dots 10^8$

ϑ	C_1/C_2	C_1/C_6	C_1/C_7
0	0.81 – 1.73	0.42 – 0.52	0.58 – 1.45
15	0.55 – 0.88	0.29 – 0.42	0.55 – 0.88
30	0.52 – 0.81	0.21 – 0.42	0.52 – 0.81
45	0.54 – 0.83	0.13 – 0.42	0.51 – 0.83
60	0.51 – 0.89	0.06 – 0.42	0.51 – 0.89
75	0.49 – 0.89	0.01 – 0.42	0.49 – 0.89
90	0.43 – 1.11	0.01 – 0.42	0.43 – 1.11

no such explicit dependence in the solution (B.11). We interpret this conflict as evidence that the isotropic ansatz for \mathcal{R}_{ij} in (22) is quite generally inadequate in view of the anisotropy induced by the direction of the rotation vector. An appropriate anisotropic

ansatz would also introduce a dependence on the rotation rate Ω_0 (or Ta). Possible additional closure terms are, e.g.

$$\begin{aligned} \Omega_i \Omega_j, \quad \mathcal{R}_{il} \Omega_l \Omega_j + \mathcal{R}_{jl} \Omega_l \Omega_i & \text{ for } \dot{\mathcal{R}}_{ij}, \\ \varepsilon_{ijk} \Omega_j \mathcal{F}_k & \text{ for } \dot{\mathcal{F}}_i, \end{aligned}$$

where all corresponding coefficients may depend on $|\mathbf{g} \cdot \boldsymbol{\Omega}|$ and/or $|\boldsymbol{\Omega}|$.

3.2.2. Reynolds stress and heat fluxes in comparison to compressible simulations

The off-diagonal Reynolds stresses and turbulent heat flux are important in generating the differential rotation of stellar convective envelopes (e.g. Rüdiger 1989). These quantities have been computed from numerous simulations of compressible convection in Cartesian (e.g. Pulkkinen et al. 1993; Chan 2001;

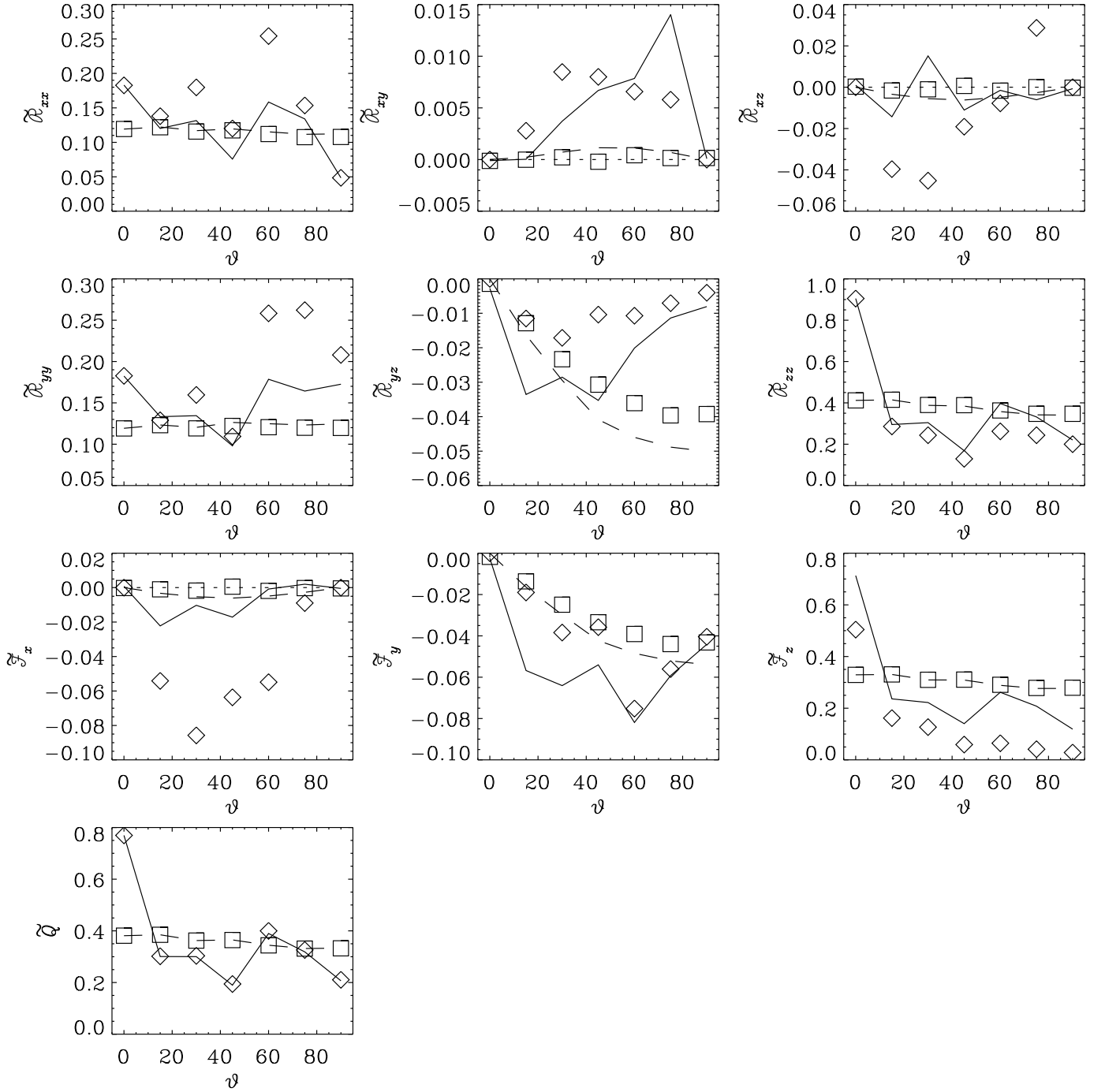


Fig. 5: Results of the closure model with coefficients $\{C_i\}$ from the optimization approach with the corresponding DNS results. Dashed lines/squares: slow rotation ($Ta = 4 \cdot 10^4$), solid lines/diamonds: faster rotation ($Ta = 1.3 \cdot 10^7$).

Käpylä et al. 2004; Rüdiger et al. 2005b) and spherical geometries (e.g. Rieutord et al. 1994; Käpylä et al. 2011). It is important to compare the results of our homogeneous Boussinesq runs to those in the literature in order to draw conclusions on the robustness of certain features such as the latitude and rotation rate dependence.

We find that \mathcal{R}_{xy} , corresponding to latitudinal flux of angular momentum is always positive, i.e. directed towards the equator in accordance with previous DNS and analytical theory (Kichatinov & Rüdiger 1993; Kichatinov & Rüdiger 2005). There is a tendency for the maximum of \mathcal{R}_{xy} to move toward the equator as the rotation rate is increased in accordance with com-

pressible simulations of Chan (2001) and Käpylä et al. (2004). Furthermore, the vertical flux corresponding to \mathcal{R}_{yz} is always negative. No sign reversal, observed at high Co in compressible runs of Käpylä et al. (2004), is seen even for the highest Taylor numbers. The third off-diagonal component \mathcal{R}_{xz} is mostly negative, although positive values occur at mid-latitudes for rapid rotation. Earlier results suggest that positive values occur at high latitudes only (e.g. Pulkkinen et al. 1993).

The latitudinal heat flux \mathcal{F}_x is always directed towards the pole and the azimuthal heat flux \mathcal{F}_y is negative, i.e. in the retrograde direction. These features are broadly in accordance with

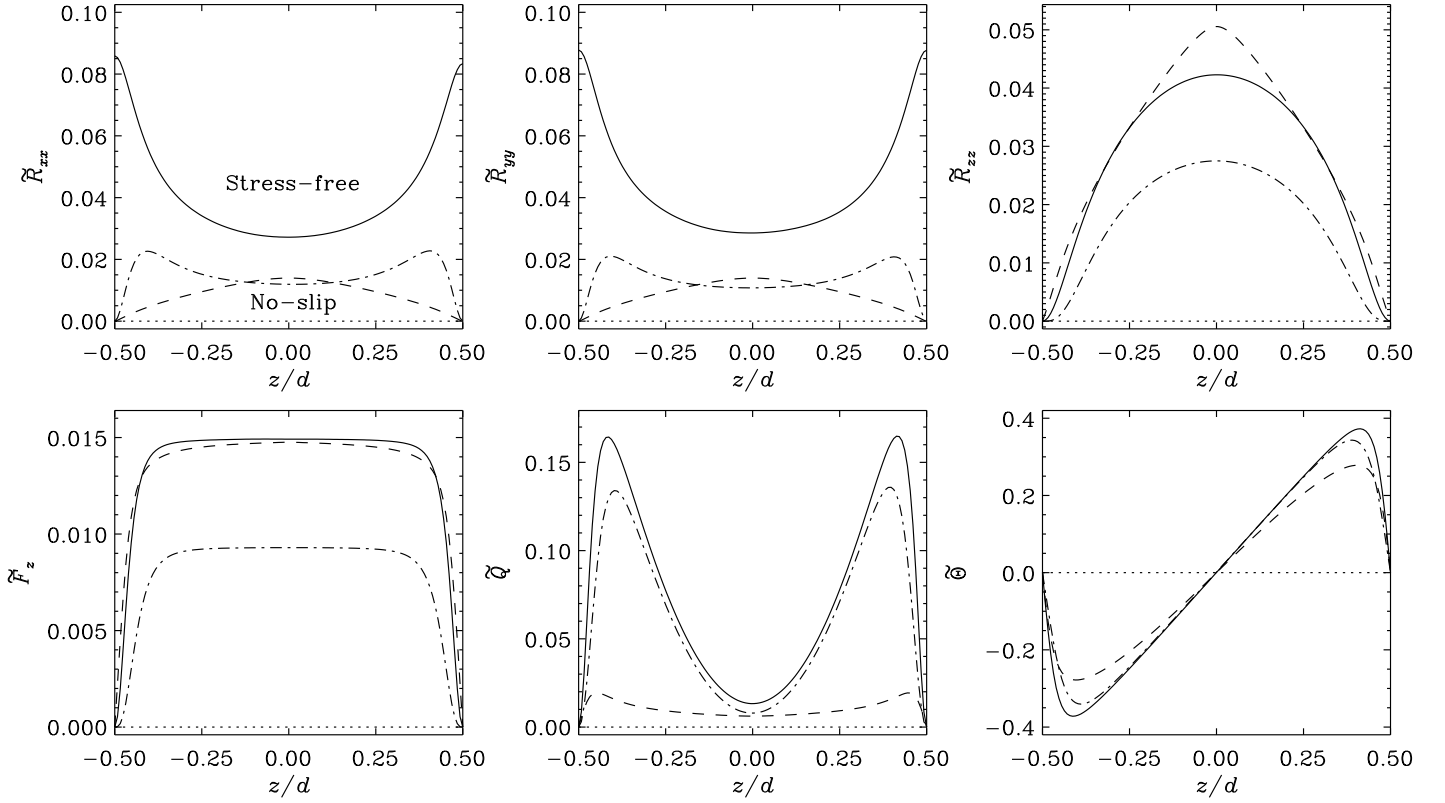


Fig. 6: Vertical profiles of the stationary solution for the inhomogeneous non-rotating case with stress free (solid lines) and no slip (dash-dotted) boundary conditions. Dashed curves: corresponding results from a representative 1D closure model with stress-free boundaries.

Cartesian (e.g. Rüdiger et al. 2005a) and spherical simulations (e.g. Käpylä et al. 2011).

3.3. Inhomogeneous case

Our numerical experiments with the inhomogeneous DNS setup included rotating runs at different latitudes as well as non-rotating runs, though only the latter will be considered in this paper. The main reason for excluding the former is that the closure and DNS results could not be brought to a satisfactory agreement already in the non-rotating case. The nature of this problem is independent of rotation and will be elaborated in the next Section.

For a good calibration of the closure model we have to require that in the statistically stationary state the vertical (z) profiles of the mean quantities from the DNS run under consideration and those from the stationary solution of the corresponding closure model should be in decent agreement. Thus, Pr and Ra (see Eqs. (12) and (13)) were set equal in both setups, an initial choice for the $\{C_i\}$ (with $C_{\nu,\kappa,\nu\kappa}$ neglected) was made and the system (20)–(24), discretized with second order difference formulae, was Euler integrated in time until a stationary state was reached. Then the z profiles were compared to those of the corresponding DNS run. As a sanity test we checked in each timestep whether the diagonal components of the Reynolds stress tensor remained positive, and terminated the run if not.

We show the results for all non-vanishing quantities, i.e. \mathcal{R}_{xx} , \mathcal{R}_{yy} , \mathcal{R}_{zz} , \mathcal{F}_z , \mathcal{Q} and Θ for two non-rotating runs (labeled Zsf and Zns) with $\text{Ra} = 5 \cdot 10^5$ and $\text{Pr} = 1$ in Fig. 6. In Run Zsf, stress-free boundary conditions (27) are applied for the velocity whereas in Run Zns, no-slip boundaries (28) are used. We per-

formed a representative 1D closure model run where the ratios of the C_i parameters were taken from the non-rotating homogeneous run (see Table 2) while we scaled C_1 so that fair agreement for \mathcal{F}_z between the DNS and closure is obtained. Stress-free boundaries are applied in the closure model. The resulting DNS vs. closure model profiles for the non-zero quantities are also shown in Fig. 6, wherefrom we see that the general forms and magnitudes of \mathcal{F}_z , Θ and \mathcal{R}_{zz} are in qualitative agreement, while the shape of the profile of \mathcal{Q} is qualitatively correct but the magnitude from the closure model is much smaller than that from DNS. The most severe discrepancy is observed for the diagonal components \mathcal{R}_{xx} and \mathcal{R}_{yy} , for which neither the profiles nor magnitudes are correctly reproduced: The DNS results form cuplike (\cup) profiles, while the profiles from the closure model resemble more caps (\cap). Although we have set C_ν , C_χ and $C_{\nu\chi}$ to zero, the basic picture stays the same even when these parameters are given non-zero values, likewise when changing the other parameters.

For stress-free boundary conditions in the DNS models the coexistence of cuplike results for \mathcal{R}_{xx} and \mathcal{R}_{yy} with caplike results for \mathcal{R}_{zz} is physically plausible: \mathcal{R}_{zz} vanishes at the boundaries because the flow cannot permeate. When descending flows hit the bottom or ascending flows hit the top, they are deflected and redistribute their kinetic energy from the vertical component to the horizontal ones which need not vanish at the boundary. Hence one would expect \mathcal{R}_{xx} and \mathcal{R}_{yy} to rise when \mathcal{R}_{zz} tends to zero near the boundaries. The situation can potentially be improved by using no-slip boundary conditions for the velocity, forcing the horizontal velocities to obtain zero values at the vertical boundaries; results from such a DNS run are shown in

Fig. 6 with dash-dotted lines. This has the desired effect near the vertical boundaries, but \mathcal{R}_{xx} and \mathcal{R}_{yy} retain their cuplike profiles away from the boundaries.

The mathematical reason why \mathcal{R}_{xx} and \mathcal{R}_{yy} from the closure model decrease near the boundaries is related to the nature of its basic ingredients: the relaxation terms of the form $C_1 \mathcal{R}^{1/2} L^{-1} \mathcal{R}_{ij}$ and the isotropization terms of the form $C_2 \mathcal{R}^{1/2} L^{-1} (\mathcal{R}_{ij} - \frac{1}{3} \delta_{ij} \mathcal{R})$. Without any other influences, the relaxation terms tend to cause the stresses to vanish, while the isotropization term forces the diagonal components of the Reynolds stress to have the same profile: Let us examine \mathcal{R}_{xx} in the stationary case ignoring the viscous terms for simplicity. Since \bar{U} vanishes in this case, we get from Eq. (A.10)

$$\mathcal{R}_{xx} = \frac{1}{3} \frac{C_2}{C_1 + C_2} \mathcal{R}, \quad (35)$$

independent of the prescription of $L(z)$. So \mathcal{R}_{xx} simply has the same profile as \mathcal{R} and for \mathcal{R}_{yy} the situation is exactly the same, making them equal and both proportional to \mathcal{R}_{zz} . Hence, all three stresses have to vanish at the boundary if only \mathcal{R}_{zz} has to do so, that is, at any impenetrable boundary. When including the closure term with C_ν , \mathcal{R}_{xx} and \mathcal{R}_{yy} are no longer proportional to \mathcal{R}_{zz} , but still vanish with it. A mechanism to transfer kinetic energy between diagonal components of the Reynolds stress tensor near the boundaries is missing in the GOMS10 model what becomes obvious if they are stress-free.

From Eq. (38) of GOMS10 it can even generally be concluded that, independent of the boundary condition for \mathbf{U} , any regular solution of the closure model must exhibit vanishing \mathcal{R} at the boundaries as long as the length L is defined as the distance to the closest boundary.

4. Conclusions

The main conclusion to be drawn from our experiences with the homogeneous Boussinesq model is that the closure parameters $\{C_i\}$ vary as functions of Taylor number and latitude what cannot be captured by a dependence on a single quantity, say, $|\Omega \cdot \mathbf{g}|$. Further, the validity of the closure degrades as the rotation rate and colatitude are increased, as indicated by the growing residuals of the parameter fits (see Figs. 2 and 4). Both facts suggest that the GOMS10 closure is essentially incomplete in the rotating case. In particular, the purely isotropic (even isotropizing) character of the closure ansatz should be revised, given the clear anisotropies which are induced by the direction of rotation. However, even in the non-rotating case we were not able to reproduce the ratios of the coefficients $\{C_i\}$ provided in GOMS10, see Table 2. This might be tracked down to the fact that in their study the coefficients were not independently determined from DNS, but adopted without change from the inhomogeneous model while only adjusting the length scale L .

We observed that positivity of the parameters and their adherence to the realizability condition alone always guarantees stability of the stationary solutions of the closure model in accordance to the stability of the underlying statistically stationary DNS solution.

In general we have not studied Rayleigh numbers higher than $Ra \approx 5 \cdot 10^5$ due to computational constraints that arise as a consequence of the higher resolution required. This might be relevant for the comparison to GOMS10 having employed up to two orders of magnitude higher values. Another aspect of potential importance for such comparison is our computational box aspect ratio of unity (they have less than unity) which nevertheless allows for statistically stationary solutions in DNS.

For the inhomogeneous setups, too, these findings keep their validity: we could not reproduce the GOMS10 results quantitatively, but our results are again limited by the moderate Rayleigh numbers. The model parameters were found to be not universal, but dependent on rotation rate and latitude. However, we abstained from presenting the latter findings in the paper as already in the non-rotating case we detected a basic difficulty: it was virtually impossible to choose model parameters such, that the profiles of \mathcal{R}_{xx} and \mathcal{R}_{yy} from the DNS could be reproduced *qualitatively* by the closure model although this was successfully demonstrated in GOMS10. As a reason for this discrepancy we could identify the stress-free boundary conditions of our model as opposed to the no-slip ones in GOMS10: by virtue of its isotropization terms, the closure ansatz is unable to model the redistribution of kinetic energy from the normal to the lateral flows close to any impenetrable boundary. This flaw is veiled for no-slip conditions because all flow components then tend to zero near the boundary, but not so for stress-free conditions. As a consequence, we obtained convex instead of concave z profiles for the mentioned Reynolds stress components being just those which do not vanish at stress-free boundaries. As a way out, terms should be added to the closure which explicitly model the named energy redistribution, that is, which are of explicit “anisotropizing” nature and are in effect only close to the boundaries. Most likely the closure model could profit from such terms for any impenetrable boundary condition.

Acknowledgements. The computations were performed on the facilities hosted by the CSC – IT Center for Science in Espoo, Finland, who are financed by the Finnish ministry of education. The authors acknowledge financial support from the Academy of Finland grant Nos. 136189, 140970 (PJK), 218159 and 141017 (MJM), and the University of Helsinki research project ‘Active Suns’. The authors acknowledge the hospitality of NORDITA. JES acknowledges the financial support from the Finnish Cultural Foundation.

Appendix A: Closure model equations for the inhomogeneous Boussinesq system

The equations for the fluctuating quantities \mathbf{u} and θ read

$$\begin{aligned} \frac{\partial \mathbf{u}}{\partial t} = & -\bar{\mathbf{U}} \cdot \nabla \mathbf{u} - \mathbf{u} \cdot \nabla \bar{\mathbf{U}} - \alpha \theta \mathbf{g} - \nabla \psi \\ & - 2 \Omega \times \mathbf{u} + \nu \nabla^2 \mathbf{u} - \nabla \cdot (\mathbf{u} \otimes \mathbf{u} - \mathcal{R}), \end{aligned} \quad (A.1)$$

$$\frac{\partial \theta}{\partial t} = -\bar{\mathbf{U}} \cdot \nabla \theta - \mathbf{u} \cdot \nabla (\bar{\Theta} + T_0) + \chi \nabla^2 \theta - \nabla \cdot (\theta \mathbf{u} - \mathcal{F}),$$

with \otimes denoting the dyadic product, or, in component form

$$\begin{aligned} \frac{\partial u_i}{\partial t} = & -\bar{U}_j \partial_j u_i - u_j \partial_j \bar{U}_i - \alpha \theta g_i - \partial_i \psi \\ & - 2 \varepsilon_{ijk} \Omega_j u_k + \nu \partial_{jj} u_i - \partial_j (u_i u_j - \mathcal{R}_{ij}), \end{aligned} \quad (A.2)$$

$$\frac{\partial \theta}{\partial t} = -\bar{U}_j \partial_j \theta - u_j \partial_j (\bar{\Theta} + T_0) + \chi \partial_{jj} \theta - \partial_j (\theta u_j - \mathcal{F}_j).$$

Apart from the Coriolis term, these equations are identical to those given in GOMS10. From them we can derive the following equations for the Reynolds stresses \mathcal{R}_{ij} , the turbulent heat flux

\mathcal{F}_i and the temperature variance \mathcal{Q}

(with $\overline{U}_z = 0$)

$$\dot{\mathcal{R}}_{ij} + \overline{U}_k \partial_k \mathcal{R}_{ij} + \mathcal{R}_{ik} \partial_k \overline{U}_j + \mathcal{R}_{jk} \partial_k \overline{U}_i + \alpha(\mathcal{F}_i g_j + \mathcal{F}_j g_i) - \nu \partial_{kk} \mathcal{R}_{ij} + 2\Omega_l (\varepsilon_{ilk} \mathcal{R}_{jk} + \varepsilon_{jlk} \mathcal{R}_{ik}) = \quad (\text{A.3})$$

$$- \overline{u_i \partial_j \psi + u_j \partial_i \psi} - \overline{u_i \partial_k (u_j u_k) + u_j \partial_k (u_i u_k)} - 2\nu \overline{\partial_k u_i \partial_k u_j},$$

$$\dot{\mathcal{F}}_i + \overline{U}_j \partial_j \mathcal{F}_i + \mathcal{F}_j \partial_j \overline{U}_i + \mathcal{R}_{ij} \partial_j (\overline{\Theta} + T_0) + \alpha \mathcal{Q} g_i - \frac{1}{2}(\nu + \chi) \partial_{jj} \mathcal{F}_i + 2\varepsilon_{ijk} \Omega_j \mathcal{F}_k = \quad (\text{A.4})$$

$$- \overline{\theta \partial_i \psi} - \overline{\theta \partial_j (u_i u_j) + u_i \partial_j (\theta u_j)} + \frac{1}{2}(\nu - \chi) \overline{\partial_k (\theta \partial_k u_i - u_i \partial_k \theta)} - (\nu + \chi) \overline{\partial_k \theta \partial_k u_i},$$

$$\dot{\mathcal{Q}} + \overline{U}_i \partial_i \mathcal{Q} + 2\mathcal{F}_i \partial_i (\overline{\Theta} + T_0) - \chi \partial_{ii} \mathcal{Q} = \quad (\text{A.5})$$

$$- 2\overline{\theta \partial_i (\theta u_i)} - 2\chi \overline{(\partial_i \theta)^2}.$$

Here, the right hand sides contain third order correlations of turbulent quantities (including the correlations with the pressure ψ) and terms originating from the Laplacians which cannot be expressed by the considered second order correlations. In the closure model of GOMS10 all these are replaced in the following way:

$$\begin{aligned} & \overline{u_i \partial_j \psi + u_j \partial_i \psi} + \overline{u_i \partial_k (u_j u_k) + u_j \partial_k (u_i u_k)} + 2\nu \overline{\partial_k u_i \partial_k u_j} \\ & \rightarrow \frac{C_1}{L} \mathcal{R}^{1/2} \mathcal{R}_{ij} + \frac{C_2}{L} \mathcal{R}^{1/2} (\mathcal{R}_{ij} - \frac{1}{3} \mathcal{R} \delta_{ij}) + \nu \frac{C_\nu}{L^2} \mathcal{R}_{ij} \\ & = \Lambda_{\mathcal{R}} \mathcal{R}_{ij} - \frac{C_2}{3L} \mathcal{R}^{3/2} \delta_{ij}, \end{aligned} \quad (\text{A.6})$$

$$\begin{aligned} & \overline{\theta \partial_i \psi} + \overline{\theta \partial_j (u_i u_j) + u_i \partial_j (\theta u_j)} \\ & - \frac{1}{2}(\nu - \chi) \overline{\partial_k (\theta \partial_k u_i - u_i \partial_k \theta)} + (\nu + \chi) \overline{\partial_k \theta \partial_k u_i} \\ & \rightarrow \frac{C_6}{L} \mathcal{R}^{1/2} \mathcal{F}_i + \frac{1}{2}(\nu + \chi) \frac{C_{\nu\chi}}{L^2} \mathcal{F}_i = \Lambda_{\mathcal{F}} \mathcal{F}_i, \end{aligned} \quad (\text{A.7})$$

$$2\overline{\theta \partial_i (\theta u_i)} + 2\chi \overline{(\partial_i \theta)^2} \rightarrow \frac{C_7}{L} \mathcal{R}^{1/2} \mathcal{Q} + \chi \frac{C_\chi}{L^2} \mathcal{Q} = \Lambda_{\mathcal{Q}} \mathcal{Q} \quad (\text{A.8})$$

with

$$\Lambda_{\mathcal{R}} = \frac{(C_1 + C_2)}{L} \mathcal{R}^{1/2} + \nu \frac{C_\nu}{L^2}, \quad (\text{A.9})$$

$$\Lambda_{\mathcal{F}} = \frac{C_6}{L} \mathcal{R}^{1/2} + \frac{1}{2}(\nu + \chi) \frac{C_{\nu\chi}}{L^2}, \quad \Lambda_{\mathcal{Q}} = \frac{C_7}{L} \mathcal{R}^{1/2} + \chi \frac{C_\chi}{L^2}.$$

Thus, the closure consists of relaxation terms, such as $C_1 L^{-1} \mathcal{R}^{1/2} \mathcal{R}_{ij}$, isotropization terms $C_2 L^{-1} \mathcal{R}^{1/2} (\mathcal{R}_{ij} - \frac{1}{3} \mathcal{R} \delta_{ij})$ and terms like $\nu C_\nu L^{-2} \mathcal{R}_{ij}$ corresponding with turbulent diffusion. For the length scale L we adopt the distance to the closest vertical boundary. Applying these simplifications we arrive at the equations (22–24). In component form they read

$$\begin{aligned} \dot{\mathcal{R}}_{xx} &= -2\mathcal{R}_{xz} \partial_z \overline{U}_x + 4\Omega_z \mathcal{R}_{xy} + \nu \partial_{zz} \mathcal{R}_{xx} \\ &\quad - \Lambda_{\mathcal{R}} \mathcal{R}_{xx} + \frac{C_2}{3L} \mathcal{R}^{3/2}, \end{aligned} \quad (\text{A.10})$$

$$\begin{aligned} \dot{\mathcal{R}}_{xy} &= -\mathcal{R}_{xz} \partial_z \overline{U}_y - \mathcal{R}_{yz} \partial_z \overline{U}_x + 2\Omega_x \mathcal{R}_{xz} \\ &\quad + 2\Omega_z (\mathcal{R}_{yy} - \mathcal{R}_{xx}) + \nu \partial_{zz} \mathcal{R}_{xy} - \Lambda_{\mathcal{R}} \mathcal{R}_{xy}, \end{aligned} \quad (\text{A.11})$$

$$\begin{aligned} \dot{\mathcal{R}}_{xz} &= -\mathcal{R}_{zz} \partial_z \overline{U}_x - \alpha \mathcal{F}_x g_z - 2\Omega_x \mathcal{R}_{xy} + 2\Omega_z \mathcal{R}_{yz} \\ &\quad + \nu \partial_{zz} \mathcal{R}_{xz} - \Lambda_{\mathcal{R}} \mathcal{R}_{xz}, \end{aligned} \quad (\text{A.12})$$

$$\begin{aligned} \dot{\mathcal{R}}_{yy} &= -2\mathcal{R}_{yz} \partial_z \overline{U}_y + 4\Omega_x \mathcal{R}_{yz} - 4\Omega_z \mathcal{R}_{xy} + \nu \partial_{zz} \mathcal{R}_{yy} \\ &\quad - \Lambda_{\mathcal{R}} \mathcal{R}_{yy} + \frac{C_2}{3L} \mathcal{R}^{3/2}, \end{aligned} \quad (\text{A.13})$$

$$\begin{aligned} \dot{\mathcal{R}}_{yz} &= -\mathcal{R}_{zz} \partial_z \overline{U}_y - \alpha \mathcal{F}_y g_z + 2\Omega_x (\mathcal{R}_{zz} - \mathcal{R}_{yy}) - 2\Omega_z \mathcal{R}_{xz} \\ &\quad + \nu \partial_{zz} \mathcal{R}_{yz} - \Lambda_{\mathcal{R}} \mathcal{R}_{yz}, \end{aligned} \quad (\text{A.14})$$

$$\begin{aligned} \dot{\mathcal{R}}_{zz} &= -2\alpha \mathcal{F}_z g_z - 4\Omega_x \mathcal{R}_{yz} + \nu \partial_{zz} \mathcal{R}_{zz} \\ &\quad - \Lambda_{\mathcal{R}} \mathcal{R}_{zz} + \frac{C_2}{3L} \mathcal{R}^{3/2}. \end{aligned} \quad (\text{A.15})$$

$$\begin{aligned} \dot{\mathcal{F}}_x &= -\mathcal{R}_{xz} \partial_z (\overline{\Theta} + T_0) - \mathcal{F}_z \partial_z \overline{U}_x + \frac{1}{2}(\nu + \chi) \partial_{zz} \mathcal{F}_x \\ &\quad + 2\Omega_z \mathcal{F}_y - \Lambda_{\mathcal{F}} \mathcal{F}_x, \end{aligned} \quad (\text{A.16})$$

$$\begin{aligned} \dot{\mathcal{F}}_y &= -\mathcal{R}_{yz} \partial_z (\overline{\Theta} + T_0) - \mathcal{F}_z \partial_z \overline{U}_y + \frac{1}{2}(\nu + \chi) \partial_{zz} \mathcal{F}_y \\ &\quad + 2\Omega_x \mathcal{F}_z - 2\Omega_z \mathcal{F}_x - \Lambda_{\mathcal{F}} \mathcal{F}_y, \end{aligned} \quad (\text{A.17})$$

$$\begin{aligned} \dot{\mathcal{F}}_z &= -\mathcal{R}_{zz} \partial_z (\overline{\Theta} + T_0) - \alpha \mathcal{Q} g_z + \frac{1}{2}(\nu + \chi) \partial_{zz} \mathcal{F}_z \\ &\quad - 2\Omega_x \mathcal{F}_y - \Lambda_{\mathcal{F}} \mathcal{F}_z, \end{aligned} \quad (\text{A.18})$$

$$\dot{\mathcal{Q}} = -2\mathcal{F}_z \partial_z (\overline{\Theta} + T_0) + \chi \partial_{zz} \mathcal{Q} - \Lambda_{\mathcal{Q}} \mathcal{Q}, \quad (\text{A.19})$$

Given that the temperature profile T_0 is linear in z and steady, the last equations and the evolution equation (19) for $\overline{\Theta}$ can be simplified by setting $\overline{\Theta} + T_0 \rightarrow \overline{\Theta}$. Then the boundary conditions for $\overline{\Theta}$ of have of course to be changed to the original ones for T . Note that the stationary version of the autonomous system (A.10)–(A.19) with (20)–(21) does have non-trivial solutions as demonstrated in GOMS10. Due to the nonlinearity of the system they exist not only for specific combinations of its parameters like in linear eigenvalue problems, but (at least within wide margins) for any specification of them.

Appendix B: Closure model equations for the homogeneous Boussinesq system

In the case with periodic boundary conditions, a further simplification consists in restricting the model to those parts of the mean quantities which are independent of z . This is equivalent to redefining the average as a volume rather than a horizontal one.

We obtain

$$\begin{aligned}
 \dot{\mathcal{R}}_{xx} &= 4\Omega_z \mathcal{R}_{xy} - \Lambda_{\mathcal{R}} \mathcal{R}_{xx} + \frac{C_2}{3L} \mathcal{R}^{3/2}, \\
 \dot{\mathcal{R}}_{xy} &= 2\Omega_x \mathcal{R}_{xz} + 2\Omega_z (\mathcal{R}_{yy} - \mathcal{R}_{xx}) - \Lambda_{\mathcal{R}} \mathcal{R}_{xy}, \\
 \dot{\mathcal{R}}_{xz} &= -\alpha \mathcal{F}_x g_z - 2\Omega_x \mathcal{R}_{xy} + 2\Omega_z \mathcal{R}_{yz} - \Lambda_{\mathcal{R}} \mathcal{R}_{xz}, \\
 \dot{\mathcal{R}}_{yy} &= 4\Omega_x \mathcal{R}_{yz} - 4\Omega_z \mathcal{R}_{xy} - \Lambda_{\mathcal{R}} \mathcal{R}_{yy} + \frac{C_2}{3L} \mathcal{R}^{3/2}, \\
 \dot{\mathcal{R}}_{yz} &= -\alpha \mathcal{F}_y g_z + 2\Omega_x (\mathcal{R}_{zz} - \mathcal{R}_{yy}) - 2\Omega_z \mathcal{R}_{xz} - \Lambda_{\mathcal{R}} \mathcal{R}_{yz}, \\
 \dot{\mathcal{R}}_{zz} &= -2\alpha \mathcal{F}_z g_z - 4\Omega_x \mathcal{R}_{yz} - \Lambda_{\mathcal{R}} \mathcal{R}_{zz} + \frac{C_2}{3L} \mathcal{R}^{3/2}, \\
 \dot{\mathcal{F}}_x &= -\mathcal{R}_{xz} G_0 + 2\Omega_z \mathcal{F}_y - \Lambda_{\mathcal{F}} \mathcal{F}_x, \\
 \dot{\mathcal{F}}_y &= -\mathcal{R}_{yz} G_0 + 2\Omega_x \mathcal{F}_z - 2\Omega_z \mathcal{F}_x - \Lambda_{\mathcal{F}} \mathcal{F}_y, \\
 \dot{\mathcal{F}}_z &= -\mathcal{R}_{zz} G_0 - \alpha \mathcal{Q} g_z - 2\Omega_x \mathcal{F}_y - \Lambda_{\mathcal{F}} \mathcal{F}_z, \\
 \dot{\mathcal{Q}} &= -2\mathcal{F}_z G_0 - \Lambda_{\mathcal{Q}} \mathcal{Q},
 \end{aligned} \tag{B.1}$$

with $G_0 = \Delta T_0 / L_z$ which is for $\Omega = 0$ equivalent to Eqs. (53) of GOMS10. The resulting equation for \mathcal{R} reads

$$\dot{\mathcal{R}} = -2\alpha \mathcal{F}_z g_z - \frac{C_1}{L} \mathcal{R}^{3/2} \tag{B.3}$$

and is not explicitly influenced by rotation.

In the non-rotating case the equations for $\dot{\mathcal{R}}_{xx}$, $\dot{\mathcal{R}}_{yy}$, $\dot{\mathcal{R}}_{zz}$, $\dot{\mathcal{F}}_z$ and $\dot{\mathcal{Q}}$ form a closed system which can be solved in separation from the remaining equations. Once the solution of the former is known the latter can be solved where one finds again two separate systems: $\{\dot{\mathcal{R}}_{xz}, \dot{\mathcal{F}}_x\}$ and $\{\dot{\mathcal{R}}_{yz}, \dot{\mathcal{F}}_y\}$. The latter two systems have the same shape, and when assuming that there is a stationary solution for \mathcal{R} from the first system, we arrive at the eigenvalue problem for the growth rate of an ansatz $\mathcal{R}_{xz}, \mathcal{F}_x, \mathcal{R}_{yz}, \mathcal{F}_y \sim \exp(\lambda t)$

$$\begin{vmatrix} \Lambda_{\mathcal{R}} + \lambda & \alpha g_z \\ G_0 & \Lambda_{\mathcal{F}} + \lambda \end{vmatrix} = 0 \tag{B.4}$$

with constant $\Lambda_{\mathcal{R}}, \Lambda_{\mathcal{F}}$. The solutions are

$$\lambda_{1,2} = -\frac{\Lambda_{\mathcal{R}} + \Lambda_{\mathcal{F}}}{2} \pm \sqrt{\frac{(\Lambda_{\mathcal{R}} - \Lambda_{\mathcal{F}})^2}{4} + \alpha g_z G_0} \tag{B.5}$$

and given that $\alpha g_z G_0 > 0$ for convection, unstable solutions cannot completely be ruled out for sufficiently large values of this product, but had most likely to be considered unphysical.

Nontrivial closed form *stationary* solutions can be derived for the special settings $\Omega = 0$ and $\vartheta = 0$ (pole): In both cases we have

$$\mathcal{R}_{xy} = \mathcal{R}_{xz} = \mathcal{R}_{yz} = \mathcal{F}_x = \mathcal{F}_y = 0, \tag{B.6}$$

$$\mathcal{R}_{xx} = \mathcal{R}_{yy} = \frac{C_2}{3L} \frac{\mathcal{R}^{3/2}}{\Lambda_{\mathcal{R}}} = \frac{C_2}{3(C_1 + C_2)} \mathcal{R} \tag{B.7}$$

hence

$$\mathcal{R} = \frac{2\alpha g_z G_0 L^2}{C_1 C_6} \left(\frac{C_1}{C_7} + \frac{3C_1 + C_2}{3(C_1 + C_2)} \right) \tag{B.8}$$

$$\mathcal{R}_{zz} = \frac{3C_1 + C_2}{3(C_1 + C_2)} \mathcal{R}, \quad \mathcal{F}_z = -\frac{C_1}{2\alpha g_z L} \mathcal{R}^{3/2} \tag{B.9}$$

$$\mathcal{Q} = \frac{G_0}{\alpha g_z} \frac{C_1}{C_7} \mathcal{R} \tag{B.10}$$

which coincides with the solution given in GOMS10. In turn it is under these conditions possible to determine the $\{C_i\}$ uniquely when $\mathcal{R}_{xx} = \mathcal{R}_{yy}$, \mathcal{R}_{zz} , \mathcal{F}_z and \mathcal{Q} are given from a DNS:

$$\begin{aligned}
 3\mathcal{R}_{xx} C_1 - (\mathcal{R}_{zz} - \mathcal{R}_{xx}) C_2 &= 0 \\
 3\mathcal{R}_{zz} C_1 + (3\mathcal{R}_{zz} - \mathcal{R}) C_2 &= -6\alpha g_z L \mathcal{F}_z / \mathcal{R}^{1/2} \\
 C_6 &= -(G_0 \mathcal{R}_{zz} + \alpha g_z \mathcal{Q}) L / \mathcal{F}_z \mathcal{R}^{1/2} \\
 C_7 &= -2G_0 L \mathcal{F}_z / \mathcal{Q} \mathcal{R}^{1/2}.
 \end{aligned} \tag{B.11}$$

Inserting (B.8) in (B.5) we obtain

$$\begin{aligned}
 (\Lambda_{\mathcal{R}} - \Lambda_{\mathcal{F}})^2 + 4\alpha g_z G_0 - (\Lambda_{\mathcal{R}} + \Lambda_{\mathcal{F}})^2 &= 4(\alpha g_z G_0 - \Lambda_{\mathcal{R}} \Lambda_{\mathcal{F}}) \\
 &= 2\alpha g_z G_0 \left(1 - \frac{C_1 + C_2}{C_7} - \frac{C_2}{3C_1} \right)
 \end{aligned} \tag{B.12}$$

the sign of which depends solely on the parameters $\{C_i\}$ and not on $\alpha g_z G_0$. Requiring (B.12) to be negative provides an additional constraint. A corresponding generalized condition, ensuring overall stability, is referred to in Sec. 3.2.1.

Another special situation is found at the equator ($\vartheta = 0$, hence $\Omega_z = 0$) where the system (B.1) decomposes into a closed one for the quantities \mathcal{R}_{xx} , \mathcal{R}_{yy} , \mathcal{R}_{yz} , \mathcal{R}_{zz} , \mathcal{F}_y , \mathcal{F}_z and \mathcal{Q} and another one for \mathcal{R}_{xy} , \mathcal{R}_{xz} and \mathcal{F}_x which can be solved once \mathcal{R} from the first system is known. The latter reads in the stationary case

$$\begin{aligned}
 0 &= 2\Omega_x \mathcal{R}_{xz} - \Lambda_{\mathcal{R}} \mathcal{R}_{xy}, \\
 0 &= -\alpha \mathcal{F}_x g_z - 2\Omega_x \mathcal{R}_{xy} - \Lambda_{\mathcal{R}} \mathcal{R}_{xz}, \\
 0 &= -\mathcal{R}_{xz} G_0 - \Lambda_{\mathcal{F}} \mathcal{F}_x,
 \end{aligned}$$

with \mathcal{F}_x being eliminated by the last line by $\mathcal{F}_x = -G_0 \mathcal{R}_{xz} / \Lambda_{\mathcal{R}}$. The remaining two equations form a homogeneous linear system for \mathcal{R}_{xy} and \mathcal{R}_{xz} having the determinant

$$\alpha g_z G_0 \frac{C_1 + C_2}{C_6} - \left(\frac{C_1 + C_2}{L} \right)^2 \mathcal{R} - 4\Omega_x^2.$$

Nontrivial solutions would be possible if \mathcal{R} were to assume a special value depending on the parameters. However, this had the unphysical consequence, that then \mathcal{R}_{xy} , \mathcal{R}_{xz} and \mathcal{F}_x would depend on an arbitrary quantity. So we have to conclude, that they either vanish or are time-dependent. In the latter case we had to require stability, so these quantities were bound to decay to zero or to perform stationary oscillations with an arbitrary amplitude. As the only physically meaningful option we assume that they vanish.

The remaining system reads

$$\begin{aligned}
 0 &= -\Lambda_{\mathcal{R}} \mathcal{R}_{xx} + \frac{C_2}{3L} \mathcal{R}^{3/2}, \\
 0 &= 4\Omega_x \mathcal{R}_{yz} - \Lambda_{\mathcal{R}} \mathcal{R}_{yy} + \frac{C_2}{3L} \mathcal{R}^{3/2}, \\
 0 &= -\alpha \mathcal{F}_y g_z + 2\Omega_x (\mathcal{R}_{zz} - \mathcal{R}_{yy}) - \Lambda_{\mathcal{R}} \mathcal{R}_{yz}, \\
 0 &= -2\alpha \mathcal{F}_z g_z - 4\Omega_x \mathcal{R}_{yz} - \Lambda_{\mathcal{R}} \mathcal{R}_{zz} + \frac{C_2}{3L} \mathcal{R}^{3/2}, \\
 0 &= -\mathcal{R}_{yz} G_0 + 2\Omega_x \mathcal{F}_z - \Lambda_{\mathcal{F}} \mathcal{F}_y, \\
 0 &= -\mathcal{R}_{zz} G_0 - \alpha \mathcal{Q} g_z - 2\Omega_x \mathcal{F}_y - \Lambda_{\mathcal{F}} \mathcal{F}_z, \\
 0 &= -2\mathcal{F}_z G_0 - \Lambda_{\mathcal{Q}} \mathcal{Q}.
 \end{aligned}$$

From the first line it follows $\mathcal{R} = C_{12}(\mathcal{R}_{yy} + \mathcal{R}_{zz})$, $C_{12} = 3(C_1 + C_2)/(3C_1 + 2C_2)$ and from the last $\mathcal{Q} = -2G_0 \mathcal{F}_z / \Lambda_{\mathcal{Q}}$ leaving a system with five variables only. It can be broken down

to a nonlinear equation for \mathcal{R} which is solved by $\mathcal{R} = 0$ and the solutions of

$$2\Omega_x(2K - \mathcal{R}E(\mathcal{R})/C_{12}) - \Lambda_{\mathcal{R}}KD(\mathcal{R}) - \alpha g_z G(\mathcal{R})E(\mathcal{R}) = 0, \quad (\text{B.13})$$

completed by

$$\begin{aligned} \mathcal{F}_z &= K\mathcal{R}^{3/2}, \quad \mathcal{F}_y = G(\mathcal{R})\mathcal{R}^{3/2}, \\ \mathcal{R}_{yy} &= \frac{\mathcal{R}}{C_{12}} - \frac{K}{E(\mathcal{R})}\mathcal{R}^{3/2}, \quad \mathcal{R}_{yz} = \frac{KD(\mathcal{R})}{E(\mathcal{R})}\mathcal{R}^{3/2}, \\ \mathcal{R}_{zz} &= \frac{K}{E(\mathcal{R})}\mathcal{R}^{3/2}, \quad K = \frac{2C_2}{3L} - \frac{C_1 + C_2}{C_{12}L}, \end{aligned}$$

with

$$\begin{aligned} E(\mathcal{R}) &= A_z(\mathcal{R})D(\mathcal{R}) + B_z(\mathcal{R}), \quad G(\mathcal{R}) = \frac{1}{K} \frac{A_z D + B_z}{A_y D + B_y}(\mathcal{R}) \\ D(\mathcal{R}) &= \alpha g_z \frac{4\Omega_x B_z(\mathcal{R}) + \Lambda_{\mathcal{R}} B_y(\mathcal{R})}{16\Omega_x^2 + \Lambda_{\mathcal{R}}^2 - \alpha g_z (4\Omega_x A_z(\mathcal{R}) - \Lambda_{\mathcal{R}} A_y(\mathcal{R}))} \\ A_y &= \frac{G_0}{\Delta} (\alpha g_z G_0 / \Lambda_{\mathcal{Q}} - \Lambda_{\mathcal{F}}), \quad B_y = -G_0 2\Omega_x / \Delta = -A_z, \\ B_z &= -G_0 \Lambda_{\mathcal{F}} / \Delta, \quad \Delta = 4\Omega_x^2 + \Lambda_{\mathcal{F}} (\Lambda_{\mathcal{F}} - \alpha g_z 2G_0 / \Lambda_{\mathcal{Q}}) \end{aligned}$$

It cannot be guaranteed that (B.13) has positive solutions for \mathcal{R} for any arbitrary set of parameters, in particular for arbitrary positive $\{C_i\}$.

In contrast, for $\Omega \neq 0$ and $\vartheta \neq 0, 90^\circ$ none of the components of \mathcal{R} and \mathcal{F} disappear and the determination of the $\{C_i\}$ from DNS results has to deal with an overdetermined system: 10 equations vs. 4 unknowns.

With respect to the realizability constraint (32), an analysis analogous to that of GOMS10, Appendix A, but with rotation included, leads to the following relation for the temporal derivative of the quantity $\mathcal{T} = X_i T_{ij} X_j = X_i (\mathcal{R}_{ij} - \mathcal{Q}^{-1} \mathcal{F}_i \mathcal{F}_j) X_j$

$$\begin{aligned} D\mathcal{T} &= (\mathcal{F} \cdot \mathbf{X})^2 \frac{\mathcal{Q}^{-1} \sqrt{\mathcal{R}}}{L} (2C_6 - C_7 - C_1 - C_2) \\ &+ \frac{C_2}{3L} \mathcal{R}^{3/2} \mathbf{X}^2 - (C_1 + C_2) \frac{\mathcal{T} \sqrt{\mathcal{R}}}{L} - \mathcal{T} \partial_k \bar{U}_k \quad (\text{B.14}) \\ &+ 2(\mathcal{F} \cdot \mathbf{X}) \mathcal{Q}^{-1} X_j T_{jk} \partial_k (\bar{\Theta} + T_0) - 4X_i \varepsilon_{ilk} \Omega_l T_{jk} X_j \end{aligned}$$

where $D = \partial_t + \bar{U}_i \partial_i$. Repeating the arguments of GOMS10 here, one finds that the realizability condition is not affected by the presence of rotation, since Ω_l in (B.14) is multiplied by the vanishing term $T_{ij} X_j$. Similarly, by retaining the model coefficients C_ν , C_κ and $C_{\nu\kappa}$ one can derive the following expression

$$\begin{aligned} D\mathcal{T} &= (\mathcal{F} \cdot \mathbf{X})^2 \frac{\mathcal{Q}^{-1} \sqrt{\mathcal{R}}}{L} \\ &\left(2C_6 - C_7 - C_1 - C_2 + \frac{2(\nu + \kappa)C_{\nu\kappa} - \kappa C_\kappa - \nu C_\nu}{L\sqrt{\mathcal{R}}} \right) \\ &+ \frac{C_2}{3L} \mathcal{R}^{3/2} \mathbf{X}^2 - (C_1 + C_2) \frac{\mathcal{T} \sqrt{\mathcal{R}}}{L} - \mathcal{T} \partial_k \bar{U}_k \\ &+ 2(\mathcal{F} \cdot \mathbf{X}) \mathcal{Q}^{-1} X_j T_{jk} \partial_k (\bar{\Theta} + T_0) - 4X_i \varepsilon_{ilk} \Omega_l T_{jk} X_j \\ &- X_i \frac{\nu C_\nu}{L^2} T_{ij} X_j, \end{aligned}$$

from which one obtains the realizability criterion

$$2C_6 - C_7 - C_1 - C_2 + \frac{2(\nu + \kappa)C_{\nu\kappa} - \kappa C_\kappa - \nu C_\nu}{L\sqrt{\mathcal{R}}} \geq 0. \quad (\text{B.15})$$

Apart from being explicitly position-dependent via $L(z)$, this criterion cannot be formulated as a condition for the model parameters alone, unlike (32). However, we can infer the two *sufficient* conditions (32) and $2(\nu + \kappa)C_{\nu\kappa} - \kappa C_\kappa - \nu C_\nu \geq 0$. With $\text{Pr} = 1$ the latter one can be written as $4C_{\nu\kappa} - C_\kappa - C_\nu \geq 0$, which is satisfied by the values $C_{\nu\kappa} \approx 6$, $C_\nu \approx 12$ and $C_\kappa \approx 2$ given in GOMS10.

References

- Brandenburg, A. 2003, Computational aspects of astrophysical MHD and turbulence, ed. Ferriz-Mas, A. & Núñez, M., 269
- Brandenburg, A. & Dobler, W. 2002, Computer Physics Communications, 147, 471
- Calzavarini, E., Doering, C. R., Gibbon, J. D., et al. 2006, Phys. Rev. E, 73, 035301
- Chan, K. L. 2001, ApJ, 548, 1102
- Garaud, P. & Ogilvie, G. I. 2005, Journal of Fluid Mechanics, 530, 145
- Garaud, P., Ogilvie, G. I., Miller, N., & Stellmach, S. 2010, MNRAS, 407, 2451
- Ghizaru, M., Charbonneau, P., & Smolarkiewicz, P. K. 2010, ApJ, 715, L133
- Käpylä, P. J. 2011, Astronomische Nachrichten, 332, 43
- Käpylä, P. J. & Brandenburg, A. 2008, A&A, 488, 9
- Käpylä, P. J., Korpi, M. J., & Tuominen, I. 2004, A&A, 422, 793
- Käpylä, P. J., Mantere, M. J., & Brandenburg, A. 2012, ApJ, 755, L22
- Käpylä, P. J., Mantere, M. J., Guerrero, G., Brandenburg, A., & Chatterjee, P. 2011, A&A, 531, A162
- Kichatinov, L. L. & Rüdiger, G. 1993, A&A, 276, 96
- Kichatinov, L. L. & Rüdiger, G. 2005, Astronomische Nachrichten, 326, 379
- Krause, F. & Rädler, K. 1980, Mean-field magnetohydrodynamics and dynamo theory, ed. Goodman, L. J. & Love, R. N.
- Lasdon, L., Waren, A., Jain, A., & Ratner, M. 1978, ACM Transactions on Mathematical Software, 4, 34
- Liljeström, A. J., Korpi, M. J., Käpylä, P. J., Brandenburg, A., & Lyra, W. 2009, Astronomische Nachrichten, 330, 92
- Miesch, M. S., Brun, A. S., & Toomre, J. 2006, ApJ, 641, 618
- Miesch, M. S. & Toomre, J. 2009, Annual Review of Fluid Mechanics, 41, 317
- Miller, N. & Garaud, P. 2007, in American Institute of Physics Conference Series, Vol. 948, Unsolved Problems in Stellar Physics: A Conference in Honor of Douglas Gough, ed. R. J. Stancliffe, G. Houdek, R. G. Martin, & C. A. Tout, 165–169
- Pulkkinen, P., Tuominen, I., Brandenburg, A., Nordlund, A., & Stein, R. F. 1993, A&A, 267, 265
- Rieutord, M., Brandenburg, A., Mangeney, A., & Drossart, P. 1994, A&A, 286, 471
- Rüdiger, G. 1989, Differential rotation and stellar convection. Sun and the solar stars, ed. Rüdiger, G.
- Rüdiger, G., Egorov, P., Kichatinov, L. L., & Küker, M. 2005a, A&A, 431, 345
- Rüdiger, G., Egorov, P., & Ziegler, U. 2005b, Astronomische Nachrichten, 326, 315
- Rüdiger, G. & Hollerbach, R. 2004, The magnetic universe : geophysical and astrophysical dynamo theory, ed. Rüdiger, G. & Hollerbach, R.
- Snellman, J. E., Brandenburg, A., Käpylä, P. J., & Mantere, M. J. 2012a, Astronomische Nachrichten, 333, 78
- Snellman, J. E., Käpylä, P. J., Korpi, M. J., & Liljeström, A. J. 2009, A&A, 505, 955
- Snellman, J. E., Rheinhardt, M., Käpylä, P. J., Mantere, M. J., & Brandenburg, A. 2012b, Phys. Scr, 86, 018406

Table B.1: Summary of the Boussinesq DNS results. Normalizations (indicated by a tilde) are carried out with $\alpha g d \Delta T_0$ for Reynolds stresses, with $\Delta T_0 (\alpha g d \Delta T_0)^{1/2}$ for heat fluxes, and with $(\Delta T_0)^2$ for temperature variance.

Run	ϑ	Ta/ 10^6	Co	Re	$\tilde{\mathcal{R}}_{xx}$	$\tilde{\mathcal{R}}_{xy}/10^{-2}$	$\tilde{\mathcal{R}}_{xz}/10^{-2}$	$\tilde{\mathcal{R}}_{yy}$	$\tilde{\mathcal{R}}_{yz}/10^{-2}$	$\tilde{\mathcal{R}}_{zz}$	$\tilde{\mathcal{F}}_x/10^{-2}$	$\tilde{\mathcal{F}}_y/10^{-2}$	$\tilde{\mathcal{F}}_z$	$\tilde{\mathcal{Q}}$
Z	—	0.00	0.00	91	0.120	−0.000	−0.001	0.120	−0.000	0.412	−0.001	−0.001	0.328	0.381
A1	0°	0.04	0.06	91	0.119	−0.013	0.025	0.119	−0.145	0.412	−0.025	−0.178	32.908	0.381
A2	0°	0.16	0.11	92	0.123	−0.030	−0.117	0.123	−0.088	0.419	−0.166	−0.095	33.322	0.386
A3	0°	0.36	0.16	95	0.127	0.009	0.006	0.128	−0.015	0.455	0.051	−0.098	36.197	0.417
A4	0°	0.64	0.21	97	0.132	−0.056	0.001	0.132	0.093	0.476	0.016	0.073	37.854	0.434
A5	0°	1.00	0.26	97	0.131	−0.021	0.022	0.131	−0.043	0.481	0.049	−0.040	38.187	0.436
A6	0°	1.44	0.31	100	0.135	0.005	0.049	0.136	0.068	0.511	0.047	0.044	40.557	0.462
A7	0°	1.96	0.35	102	0.141	0.007	−0.054	0.141	−0.167	0.545	−0.036	−0.121	43.206	0.489
A8	0°	2.56	0.38	107	0.149	0.026	0.108	0.150	0.164	0.598	0.122	0.135	47.195	0.530
A9	0°	4.00	0.46	110	0.156	0.041	0.133	0.155	−0.185	0.649	0.127	−0.207	51.175	0.569
A10	0°	5.76	0.45	136	0.198	0.020	−0.098	0.199	−0.067	1.059	−0.132	−0.059	83.611	0.891
A11	0°	7.84	0.59	120	0.171	0.003	0.151	0.171	−0.011	0.786	0.158	−0.006	61.937	0.676
A12	0°	10.24	0.66	123	0.178	−0.047	−0.066	0.177	−0.187	0.844	−0.090	−0.162	66.429	0.721
A13	0°	12.96	0.72	127	0.183	−0.011	0.098	0.182	−0.278	0.905	0.075	−0.248	71.310	0.770
B1	15°	0.04	0.06	91	0.122	−0.001	−0.159	0.123	−1.289	0.415	−0.099	−1.364	33.088	0.385
B2	15°	0.16	0.11	89	0.116	0.011	−0.157	0.119	−2.250	0.387	−0.166	−2.361	30.883	0.361
B3	15°	0.36	0.17	89	0.115	0.079	−0.419	0.122	−3.371	0.386	−0.484	−3.643	30.926	0.362
B4	15°	0.64	0.23	87	0.112	0.161	−0.762	0.124	−4.115	0.365	−0.871	−4.506	29.146	0.345
B5	15°	1.00	0.29	86	0.111	0.288	−1.104	0.125	−4.691	0.350	−1.361	−5.201	28.112	0.337
B6	15°	1.44	0.36	84	0.109	0.352	−1.230	0.124	−4.723	0.328	−1.620	−5.342	26.442	0.320
B7	15°	1.96	0.42	84	0.109	0.377	−1.512	0.125	−4.824	0.320	−1.996	−5.539	25.875	0.315
B8	15°	2.56	0.49	83	0.108	0.318	−1.508	0.124	−4.581	0.314	−2.021	−5.391	25.412	0.310
B9	15°	4.00	0.63	81	0.107	0.282	−1.553	0.123	−4.266	0.288	−2.268	−5.362	23.460	0.292
B10	15°	5.76	0.74	82	0.112	0.215	−1.670	0.127	−4.042	0.296	−2.504	−5.360	24.033	0.300
B11	15°	7.84	0.86	83	0.115	0.082	−1.558	0.129	−3.769	0.296	−2.351	−5.390	23.986	0.301
B12	15°	10.24	0.97	83	0.118	0.061	−1.597	0.132	−3.583	0.298	−2.421	−5.560	24.023	0.303
B13	15°	12.96	1.09	83	0.120	0.003	−1.431	0.133	−3.355	0.295	−2.225	−5.678	23.610	0.301
C1	30°	0.04	0.06	89	0.116	0.022	−0.103	0.119	−2.333	0.390	−0.175	−2.492	30.992	0.362
C2	30°	0.16	0.12	86	0.110	0.093	−0.470	0.120	−3.776	0.352	−0.531	−4.210	28.265	0.336
C3	30°	0.36	0.19	80	0.099	0.277	−0.587	0.114	−4.365	0.289	−0.787	−5.068	23.388	0.286
C4	30°	0.64	0.27	76	0.093	0.420	−1.024	0.113	−4.572	0.253	−1.319	−5.596	20.598	0.259
C5	30°	1.00	0.34	74	0.091	0.561	−1.261	0.110	−4.293	0.232	−1.762	−5.499	19.107	0.244
C6	30°	1.44	0.42	72	0.088	0.597	−1.430	0.108	−3.892	0.214	−2.089	−5.415	17.695	0.230
C7	30°	1.96	0.50	71	0.088	0.594	−1.621	0.105	−3.599	0.203	−2.399	−5.272	16.736	0.221
C8	30°	2.56	0.58	70	0.088	0.531	−1.565	0.104	−3.263	0.200	−2.350	−5.005	16.327	0.217
C9	30°	4.00	0.72	70	0.091	0.487	−1.389	0.103	−2.862	0.196	−2.429	−4.908	15.826	0.213
C10	30°	5.76	0.84	73	0.098	0.455	−1.177	0.108	−2.732	0.212	−2.413	−5.026	16.781	0.228
C11	30°	7.84	0.96	74	0.104	0.383	−0.468	0.110	−2.560	0.220	−2.050	−5.137	16.980	0.233
C12	30°	10.24	1.02	80	0.118	0.362	0.377	0.123	−2.702	0.262	−1.622	−5.732	19.603	0.266
C13	30°	12.96	1.07	85	0.132	0.371	1.511	0.135	−2.855	0.304	−1.028	−6.407	22.199	0.300
D1	45°	0.04	0.06	89	0.117	−0.021	0.063	0.122	−3.071	0.389	0.054	−3.341	31.062	0.365
D2	45°	0.16	0.12	82	0.101	0.157	−0.449	0.119	−4.722	0.305	−0.527	−5.426	24.713	0.301
D3	45°	0.36	0.20	75	0.089	0.405	−0.635	0.113	−4.609	0.239	−0.885	−5.861	19.624	0.249
D4	45°	0.64	0.29	69	0.081	0.587	−0.986	0.105	−4.082	0.196	−1.401	−5.646	16.194	0.213
D5	45°	1.00	0.39	65	0.075	0.705	−1.168	0.097	−3.566	0.165	−1.822	−5.472	13.759	0.187
D6	45°	1.44	0.47	64	0.074	0.755	−1.218	0.094	−3.145	0.158	−1.982	−5.180	13.013	0.180
D7	45°	1.96	0.57	62	0.073	0.776	−1.194	0.089	−2.765	0.146	−2.095	−4.930	11.925	0.169
D8	45°	2.56	0.65	62	0.075	0.735	−1.050	0.087	−2.470	0.144	−2.061	−4.689	11.587	0.166
D9	45°	4.00	0.75	68	0.089	0.755	−0.618	0.099	−2.501	0.177	−1.944	−5.246	13.726	0.196
D10	45°	5.76	0.83	74	0.104	0.701	0.183	0.110	−2.450	0.215	−1.415	−5.606	16.019	0.228
D11	45°	7.84	0.86	83	0.128	0.738	1.376	0.131	−2.688	0.282	−0.721	−6.584	20.468	0.286
D12	45°	10.24	0.89	91	0.152	0.816	2.599	0.152	−2.936	0.348	−0.114	−7.675	24.670	0.343
D13	45°	12.96	1.39	66	0.076	0.677	−1.131	0.098	−3.511	0.169	−1.734	−5.371	14.012	0.190
E1	60°	0.04	0.06	87	0.112	0.042	−0.168	0.121	−3.609	0.363	−0.190	−3.910	29.059	0.344
E2	60°	0.16	0.13	77	0.091	0.175	−0.350	0.114	−4.614	0.259	−0.460	−5.583	21.095	0.263
E3	60°	0.36	0.22	69	0.078	0.399	−0.549	0.105	−4.219	0.194	−0.791	−5.760	16.072	0.211
E4	60°	0.64	0.32	63	0.068	0.595	−0.712	0.097	−3.530	0.150	−1.172	−5.590	12.584	0.174
E5	60°	1.00	0.43	59	0.063	0.690	−0.781	0.087	−2.856	0.128	−1.355	−5.060	10.734	0.154
E6	60°	1.44	0.53	57	0.060	0.738	−0.729	0.081	−2.384	0.115	−1.364	−4.700	9.379	0.139
E7	60°	1.96	0.60	59	0.064	0.748	−0.565	0.084	−2.232	0.123	−1.330	−4.817	9.763	0.146
E8	60°	2.56	0.67	61	0.070	0.819	−0.510	0.087	−2.015	0.135	−1.257	−4.653	10.379	0.156
E9	60°	4.00	0.76	67	0.084	0.781	−0.243	0.101	−1.838	0.170	−0.851	−4.983	12.298	0.185
E10	60°	5.76	0.82	74	0.101	0.906	−0.135	0.118	−1.880	0.213	−0.872	−5.667	15.029	0.226
E11	60°	7.84	0.87	82	0.120	0.809	0.087	0.138	−1.913	0.268	−0.317	−6.481	18.542	0.278
E12	60°	10.24	0.90	90	0.140	0.925	−0.002	0.160	−2.037	0.336	−0.390	−7.392	22.716	0.337
E13	60°	12.96	0.95	96	0.158	0.784	−0.150	0.179	−2.009	0.397	−0.083	−8.190	26.151	0.390

Table B.2: Summary of the Boussinesq DNS results continued. For explanations see Table B.1.

Run	ϑ	Ta/ 10^6	Co	Re	$\tilde{\mathcal{R}}_{xx}$	$\tilde{\mathcal{R}}_{xy}/10^{-2}$	$\tilde{\mathcal{R}}_{xz}/10^{-2}$	$\tilde{\mathcal{R}}_{yy}$	$\tilde{\mathcal{R}}_{yz}/10^{-2}$	$\tilde{\mathcal{R}}_{zz}$	$\tilde{\mathcal{F}}_x/10^{-2}$	$\tilde{\mathcal{F}}_y/10^{-2}$	$\tilde{\mathcal{F}}_z$	\tilde{Q}
F1	75°	0.04	0.06	85	0.108	0.015	0.001	0.120	-3.963	0.347	-0.028	-4.396	27.848	0.331
F2	75°	0.16	0.13	75	0.089	0.089	-0.175	0.114	-4.675	0.246	-0.187	-5.806	20.114	0.253
F3	75°	0.36	0.23	66	0.071	0.287	-0.332	0.104	-4.106	0.171	-0.493	-5.951	14.343	0.193
F4	75°	0.64	0.33	60	0.061	0.366	-0.314	0.094	-3.267	0.134	-0.575	-5.607	11.250	0.160
F5	75°	1.00	0.44	57	0.055	0.467	-0.366	0.086	-2.566	0.115	-0.674	-5.068	9.405	0.140
F6	75°	1.44	0.56	54	0.051	0.544	-0.327	0.078	-1.966	0.100	-0.659	-4.454	7.918	0.123
F7	75°	1.96	0.64	55	0.053	0.659	-0.399	0.081	-1.683	0.107	-0.701	-4.287	8.072	0.127
F8	75°	2.56	0.72	56	0.057	0.812	-0.516	0.084	-1.432	0.111	-0.770	-4.133	8.055	0.130
F9	75°	4.00	0.84	60	0.067	1.007	-0.519	0.093	-1.075	0.127	-0.686	-3.948	8.733	0.144
F10	75°	5.76	0.89	69	0.085	1.218	-0.495	0.112	-1.113	0.175	-0.518	-4.467	11.654	0.187
F11	75°	7.84	0.93	76	0.102	1.241	-0.473	0.132	-1.203	0.227	-0.229	-5.079	14.846	0.233
F12	75°	10.24	0.98	83	0.118	1.241	-0.693	0.147	-1.240	0.279	-0.171	-5.637	17.673	0.276
F13	75°	12.96	1.02	89	0.134	1.402	-0.606	0.164	-1.138	0.332	0.196	-5.919	20.774	0.319
G1	90°	0.04	0.06	85	0.108	0.015	-0.025	0.120	-3.925	0.347	-0.046	-4.319	27.933	0.332
G2	90°	0.16	0.14	75	0.087	0.010	-0.064	0.114	-4.725	0.240	-0.073	-5.925	19.723	0.250
G3	90°	0.36	0.23	66	0.069	-0.012	0.004	0.107	-4.144	0.168	-0.008	-6.277	14.067	0.192
G4	90°	0.64	0.34	60	0.058	-0.010	-0.002	0.094	-3.097	0.130	-0.018	-5.476	10.860	0.155
G5	90°	1.00	0.46	55	0.050	-0.029	0.045	0.084	-2.366	0.108	0.053	-4.896	8.771	0.132
G6	90°	1.44	0.57	53	0.045	0.004	0.018	0.082	-1.870	0.098	0.028	-4.503	7.543	0.119
G7	90°	1.96	0.68	52	0.040	0.036	-0.020	0.085	-1.381	0.090	-0.067	-4.045	6.579	0.109
G8	90°	2.56	0.85	48	0.026	0.015	0.013	0.086	-0.753	0.068	-0.003	-2.888	4.573	0.083
G9	90°	4.00	0.93	54	0.032	-0.032	0.054	0.103	-0.725	0.098	0.075	-2.992	5.823	0.103
G10	90°	5.76	0.98	62	0.039	-0.017	0.032	0.128	-0.811	0.135	0.029	-3.692	7.680	0.133
G11	90°	7.84	1.09	65	0.038	-0.009	0.025	0.143	-0.640	0.153	0.010	-3.738	8.229	0.146
G12	90°	10.24	1.16	70	0.042	-0.001	-0.021	0.161	-0.677	0.184	0.059	-4.100	9.925	0.174
G13	90°	12.96	1.22	75	0.048	0.008	-0.070	0.173	-0.806	0.220	-0.045	-4.411	11.906	0.207